Guide to animation and user-controlled Relawavity graphics on AMOP DVD

It has been traditional for the AMOP Handbook to order first the more fundamental and elementary chapters. The following is a unique electronic presentation of the most fundamental pillars underlying all of modern physics, namely *quantum theory* originated by Planck (1900) and *special relativity* originated by Einstein (1905).

Relativity and quantum theory are now an established part of popular culture. They appear in a famous movie (screenshot in Fig. 1) based on a hilarious answer to Fermi's famous SETI question, "Why *is* it so quiet out there?" The movie, *Men in Black* assumes it is *not*! Rather secret black-suited immigration officers manage a ribald alien population from within an enormous intergalactic spaceport hidden in Manhattan.

Fig. 1 1997 MIB Screenshot of first-grader, Suzy, carrying her AMOP homework.

An opening scene of MIB has the protagonist (played by Will Smith) undergo a simulated gun fight to see if he can quickly distinguish alien from innocent, whereupon he shoots little Suzy for carrying relativity and quantum physics texts. Asked why, he answers, "…clearly up to no good!"

As silly as MIB is, it provides a profound lesson about postmodern physics and how its intellectual property is to be created and transferred. Most of us grow up finding books to be intellectually richer than their screenplays. MIB, however, would be a flop as a book. Its dynamics and humor would be lost on static ink and paper.

As will be shown below, relativity and quantum theory have much to gain if presented in motion by computer animation. Both are a story about light waves in space and time. The time has come to let the light waves tell their own story more clearly using several active space-time displays combined with per-space-time (ω,ck) controls.

One outcome of this is a realization that relativity and quantum theory make much more sense if presented as the *same subject*. Separately, they each have unnecessary conundrums that resolve when combined into a subject we have named *Relawavity*. Thinking in a wavelike way changes concepts such as Lagrangian or Hamiltonian from graduate student nightmares into simple ruler&compass trigonometry, all while making trigonometry fun to learn.

Perhaps Suzy would be better off with just one book and a lighter one at that. We can speculate that future AMOP Handbooks may be made lighter than the current version, and perhaps contain a virtual reality viewer.

Space-time Cartesian wave-zero-grids

The sum $\Psi=e^{iR}+e^{iL}$ of two CW (Continuous Wave) laser beams trace (*x,ct*)-space-time grids shown in Fig. 2, an animated view of a λ=0.5μm laser cavity mode for an (*n=2*)-mode at 600THz. White lines are real zeros found by factoring sum Ψ into a *phase* factor labeled by vector **P** or $\mathbb{P}$ and a *group* wave factor labeled by vector **G** or $\mathbb{G}$.

$$\Psi=e^{iR}+e^{iL}=e^{i\frac{R+L}{2}}\left(e^{i\frac{R-L}{2}}+e^{-i\frac{R-L}{2}}\right)=e^{i\frac{R+L}{2}}2\cos\tfrac{R-L}{2}\text{ where: }R=kx-\omega t\text{ and: }L=-kx-\omega t\text{, with:}\tfrac{\omega}{2\pi}=\tfrac{ck}{2\pi}=600THz$$
$$=e^{-i\omega t}2\cos kx=\psi_{phase}\psi_{group}\text{ and:}\mathbf{P}=\frac{\mathbf{R+L}}{2}=\begin{pmatrix}\omega\\0\end{pmatrix},\ \mathbf{G}=\frac{\mathbf{R-L}}{2}=\begin{pmatrix}0\\ck\end{pmatrix}\qquad(1)$$

P and **G** vectors in reciprocal (*ck,ω*) wavevector-frequency per-space-time define space-time $\mathbb{P}$ and $\mathbb{G}$ vectors. Zero slope of **G** maps to zero group velocity on $\mathbb{G}$. Infinite slope of **P** maps to infinite phase velocity along $\mathbb{P}$.

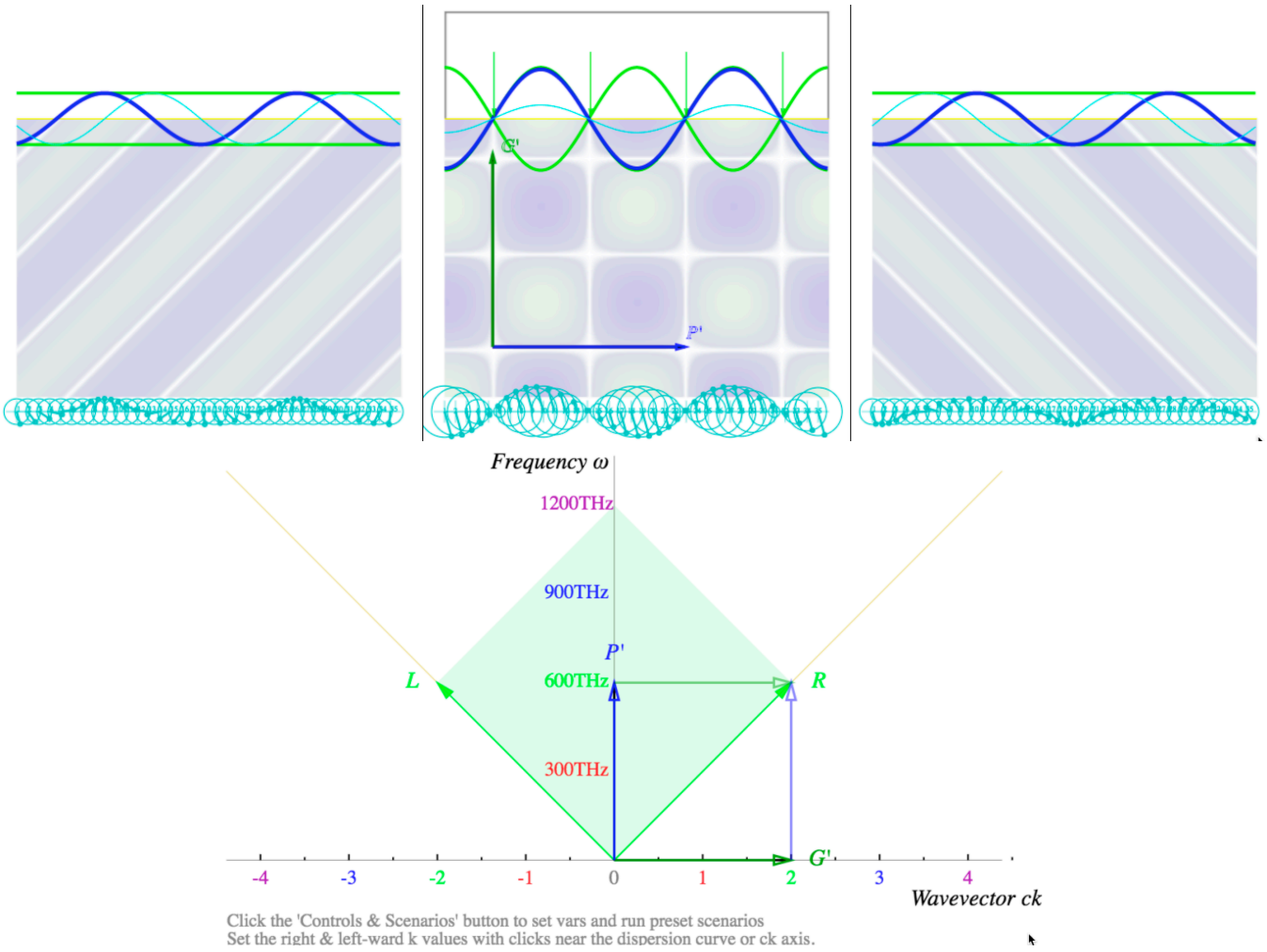

Fig. 2 Rest (x,ct) frame Cartesian grid for colliding pair of 600THz continuous waves.

Web Simulation - RelaWavity: Time-Space plots - Minkowski coordinates w/ zero tracers, β = u/c = 0
Clicking the *Wavevector ck* axis near a *positive* integer shifts that n-mode for the *Right*-moving (*R*) CW.
Clicking the *Wavevector ck* axis near a *negative* integer shifts that n-mode for the *Left*-moving (*L*) CW.

The result is generally a Minkowski (*x,ct*) grid that has non-zero group velocity and so is not a rest-frame. Fig. 3 below shows a frame traveling to the right with a wave group velocity of *u=3c/5* as is derived below the figure.

Space-time Minkowski wave-zero-grids

Let Doppler factor $e^{\rho}=2$ blue-shift R-wave to 1200THZ. This implies a red-shift of L-wave by inverse $e^{-\rho}=½$ to 300THz. Right moving R-wave has velocity $+c$ so $\omega_R=+ck_R$. Left moving L-wave has velocity $-c$ so $\omega_L=-ck_L$. Both frequency ω and k-vector must shift in concert to maintain CW light speed c.

$$\Psi=e^{iR}+e^{iL}=e^{i\frac{R+L}{2}}\left(e^{i\frac{R-L}{2}}+e^{-i\frac{R-L}{2}}\right)=e^{i\frac{R+L}{2}}2\cos\tfrac{R-L}{2} \quad \text{where: } R=k_R x-\omega_R t=e^{\rho}(kx-\omega t) \quad \text{and: } L=-k_L x-\omega_L t=e^{-\rho}(-kx-\omega t)$$

$$=\psi_{phase}\psi_{group} \quad \text{and:} \quad \mathbf{P}'=\frac{\mathbf{R}'+\mathbf{L}'}{2}=\begin{pmatrix}\frac{\omega_R+\omega_L}{2}\\ \frac{\omega_R-\omega_L}{2}\end{pmatrix}=\omega\begin{pmatrix}\frac{e^{\rho}+e^{-\rho}}{2}\\ \frac{e^{\rho}-e^{-\rho}}{2}\end{pmatrix}, \quad \mathbf{G}'=\frac{\mathbf{R}'-\mathbf{L}'}{2}=\begin{pmatrix}\frac{\omega_R-\omega_L}{2}\\ \frac{\omega_R+\omega_L}{2}\end{pmatrix}=\omega\begin{pmatrix}\frac{e^{\rho}-e^{-\rho}}{2}\\ \frac{e^{\rho}+e^{-\rho}}{2}\end{pmatrix}, \quad (2)$$

$$=\omega\begin{pmatrix}\cosh\rho\\ \sinh\rho\end{pmatrix}=\omega\begin{pmatrix}\frac{5}{4}\\ \frac{3}{4}\end{pmatrix}, \qquad =\omega\begin{pmatrix}\sinh\rho\\ \cosh\rho\end{pmatrix}=\omega\begin{pmatrix}\frac{3}{4}\\ \frac{5}{4}\end{pmatrix}.$$

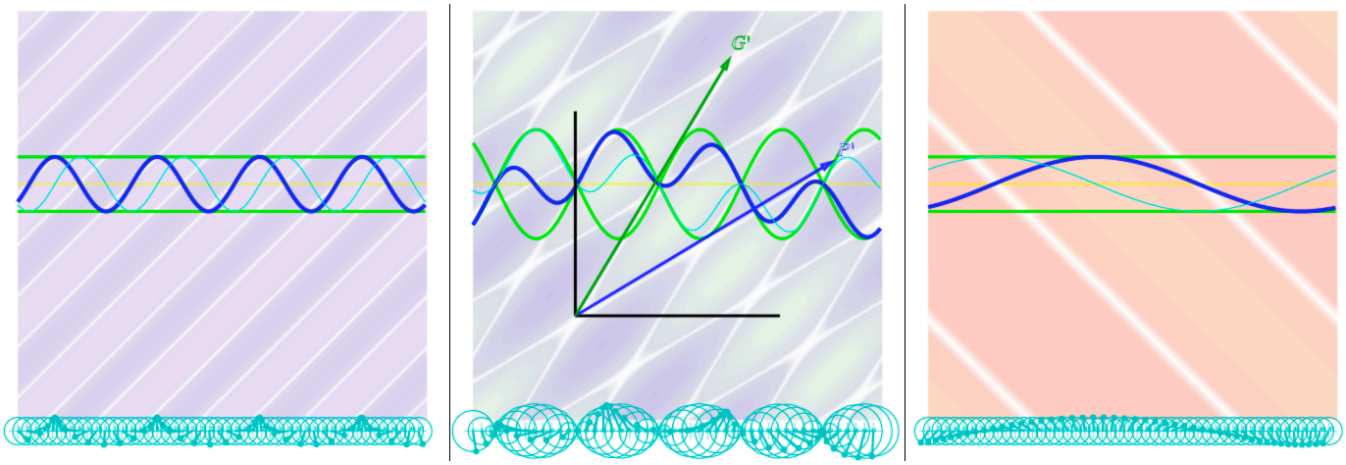

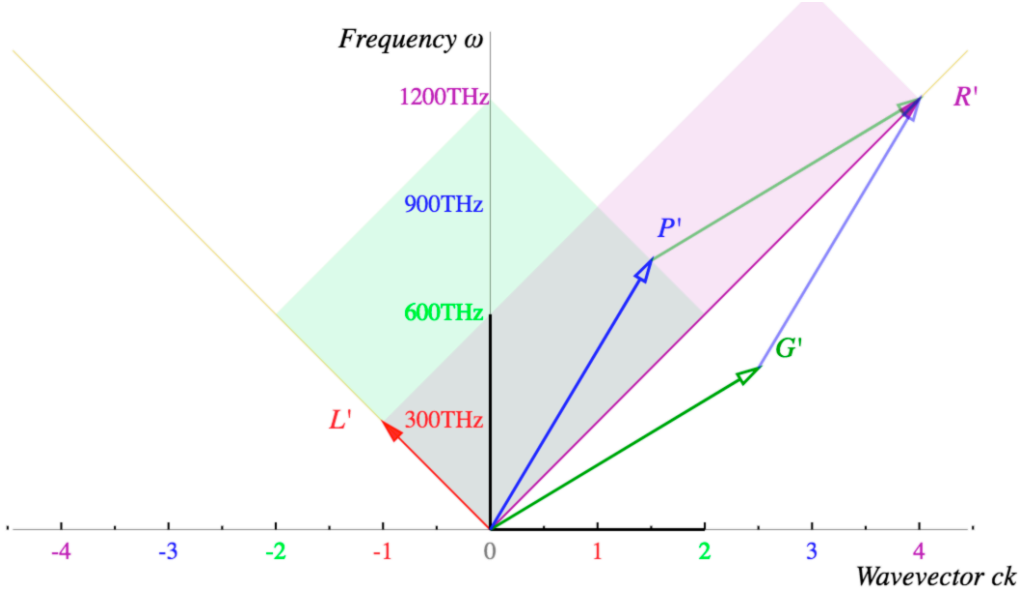

Fig. 3 Minkowski (x,ct)-frame grid for colliding pair of R=1200THz and L=300THz waves.
Web Simulation - RelaWavity: Time-Space plots - Minkowski grid w/insert of shifted axis , β = u/c = 3/5

Fig. 3 grid moves left-to-right at group velocity *3c/5,* the slope of **G** versus *ck*-axis or 𝔾 versus *ct*-axis.

$$\frac{V_{group}}{c}=\frac{\sinh\rho}{\cosh\rho}=\tanh\rho=\frac{3}{5} \quad (\mathbf{G}\text{-slope}) \quad (3a) \qquad \frac{V_{phase}}{c}=\frac{\cosh\rho}{\sinh\rho}=\coth\rho=\frac{5}{3} \quad (\mathbf{P}\text{-slope}) \quad (3b)$$

Details of Fig. 3 in Fig. 4 show 16 group and phase wave parameters listed in Table 1. This begins with Doppler shifts $e^{\pm\rho}$ and wave velocities given as functions of rapidity ρ or the well known $\beta=\frac{u}{c}$ ratio. Numerical values for case $\beta=\frac{3}{5}$ occupy the lowest row of Table 1 (See also Tables 2a-b on p.22).

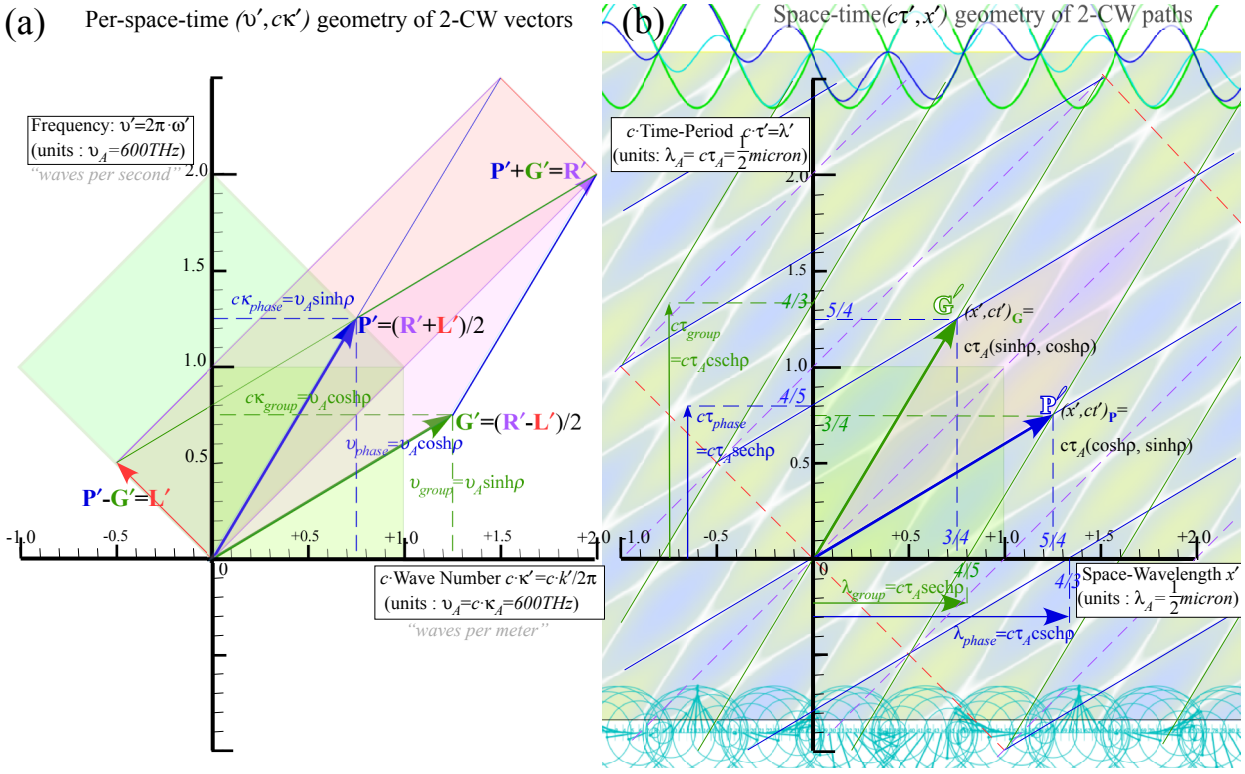

Fig. 4. Relawavity parameters given as ρ-functions as they appear in (a) Per-space-time and (b) Space-time

Table 1. Relawavity parameter formulae. Last row gives numeric values for blue-shift $b^{Doppler}_{BLUE}=2$ or $\beta=\frac{u}{c}=\frac{3}{5}$

phase	$b^{Doppler}_{RED}$	$\frac{c}{V_{phase}}$	$\frac{\kappa_{phase}}{\kappa_A}$	$\frac{\tau_{phase}}{\tau_A}$	$\frac{\upsilon_{phase}}{\upsilon_A}$	$\frac{\lambda_{phase}}{\lambda_A}$	$\frac{V_{phase}}{c}$	$b^{Doppler}_{BLUE}$
group	$\frac{1}{b^{Doppler}_{BLUE}}$	$\frac{V_{group}}{c}$	$\frac{\upsilon_{group}}{\upsilon_A}$	$\frac{\lambda_{group}}{\lambda_A}$	$\frac{\kappa_{group}}{\kappa_A}$	$\frac{\tau_{group}}{\tau_A}$	$\frac{c}{V_{group}}$	$\frac{1}{b^{Doppler}_{RED}}$
rapidity ρ	$e^{-\rho}$	$\tanh\rho$	$\sinh\rho$	$\operatorname{sech}\rho$	$\cosh\rho$	$\operatorname{csch}\rho$	$\coth\rho$	$e^{+\rho}$
$\beta\equiv\frac{u}{c}$	$\sqrt{\frac{1-\beta}{1+\beta}}$	$\frac{\beta}{1}$	$\frac{1}{\sqrt{\beta^{-2}-1}}$	$\frac{\sqrt{1-\beta^2}}{1}$	$\frac{1}{\sqrt{1-\beta^2}}$	$\frac{\sqrt{\beta^{-2}-1}}{1}$	$\frac{1}{\beta}$	$\sqrt{\frac{1+\beta}{1-\beta}}$
value for β=3/5	$\frac{1}{2}=0.5$	$\frac{3}{5}=0.6$	$\frac{3}{4}=0.75$	$\frac{4}{5}=0.80$	$\frac{5}{4}=1.25$	$\frac{4}{3}=1.33$	$\frac{5}{3}=1.67$	$\frac{2}{1}=2.0$

Web Simulations - RelaWavity: Time-Space, Per-space-time, space-time, and tabular display of Relawavity parameters
RelativIt App: Space-space and time-space plots of passing ship and lighthouses (Lighthouse frame)
RelativIt App: Space-space and time-space plots of passing ship and lighthouses (Ship frame)

Column-*(1+n)* is inverse to column-*(8-n)* for $n<8$. Two ratios in Table 1 are famous: *Lorentz x-contraction* ($\operatorname{sech}\rho=\frac{4}{5}$) or *Einstein t-dilation* ($\cosh\rho=\frac{5}{4}$) and seen in Fig. 4b as $\frac{4}{5}$- reduced *x*-spacing or $\frac{5}{4}$- increased *ct*-ordinate. However, all eight wave sizes (κ_{phase} to τ_{group}) serve equally to clearly define geometry of (*x*,*ct*) or (*cκ*,*υ*) in Fig. 4a-b and the wave dynamics that leads to quantum theory.

Thales-Euclid means and geometry of hyperbolic invariants

Imagine you detect counter-propagating laser beams of frequency ω_R going left-to-right and ω_L going right-to-left. Consider two questions:

(1.) To what velocity u_E must you accelerate to see beams with equal frequency ω_E?

(2.) What is that frequency ω_E ?

Query (1.) has a Jeopardy-style answer-by-question: What beam group velocity do you see?

$$u_E = V_{group} = \frac{\omega_{group}}{k_{group}} = \frac{\omega_R - \omega_L}{k_R - k_L} = c\frac{\omega_R - \omega_L}{\omega_R + \omega_L} \tag{4}$$

Query (2.) similarly: What ω_E is blue-shift $b\omega_L$ of ω_L *and* red-shift ω_R/b of ω_R ?

$$\omega_E = b\,\omega_L = \omega_R/b \quad \Rightarrow \quad b = \sqrt{\omega_R/\omega_L} \quad \Rightarrow \quad \omega_E = \sqrt{\omega_R \cdot \omega_L} \tag{5}$$

V_{group}/c is ratio of difference mean $\omega_{group} = \frac{\omega_R - \omega_L}{2}$ to arithmetic mean $\omega_{phase} = \frac{\omega_R + \omega_L}{2}$. Frequency $\omega_E = B$ is the geometric mean $\sqrt{\omega_R \cdot \omega_L}$ of left and right-moving frequencies defining the geometry in Fig.4 as detailed in Fig.5a. Line sum of $\omega_L = \omega_E\, e^{-\rho}$ and $\omega_L = \omega_E\, e^{+\rho}$ is bisected at center C of a circle connecting shifted phase vector $\mathbf{P}'$ to its $\sqrt{\omega_R \cdot \omega_L}$ original $\mathbf{P}$.

Original $\mathbf{P}$ ($\mathbf{P}$itcher's mound) is the geometric mean point $\sqrt{1 \cdot 4} = 2$ at Alice's base frequency of $B = v_A = 600$THz. (Fig.5 units are 300 THz.). That lets you construct points $\mathbf{P}'$, $\mathbf{P}''$, $\mathbf{P}'''$,... on a hyperbola that all frames will claim to also be their 600 THz invariant curve. Geometry begins by choosing to prick a $\mathbf{C}$-point ck' with compass needle. Then compass pencil is set to point-$\mathbf{P}$, and arc $\mathbf{P}\,\mathbf{P}'$ is drawn to the next hyperbola point $\omega'(k')$ on the new axis ck'. (Arc is optional if graph paper locates vertical $\mathbf{P}'\mathbf{C}$ line.)

Time-symmetry axiom ($e^{-\rho}\, e^{+\rho} = r \cdot b = 1$) implies phase points $\mathbf{P}'$, $\mathbf{P}''$, $\mathbf{P}'''$,… lie upon equilateral hyperbolas ($xy = const.$ or $\omega_{R'}\omega_{L'} = \omega_A^2$) whose ±45° asymptotes frame Doppler-shifted rectangles that all have the same area $2\omega_A^2$ of the initial ($\rho = 0$) baseball diamond in Fig.4a and Fig. 2. Fig. 5b shows plots of upper branches for two (ω', ck')-hyperbolas belonging to constants $\omega_A = 2$ and $\omega_A = 4$. This oblique ±45° view of the invariant hyperbolas emphasizes the Doppler shift ($r \cdot b = const.$) relations that are not immediately obvious from the usual straight-up Cartesian invariant equation such as $\omega_A^2 = \omega'^2 - c^2 k'^2$.

The geometry behind Fig. 5a or Fig. 5b is ancient and goes back to Thales of Miletus (*circa 600BCE*) about three centuries before Euclid. Thales construction of means follows from his proof by symmetry that each point on a circle subtends a right (90°) angle which in turn is based on inscribed rectangles (dashed lines in Fig. 5a). The same geometry applies to half-sum and half differences of phase angles involved in the wave interference sum sketched in Fig. 5c for each pair of phasors added in Fig. 5d. That is the geometry of factoring equations (1) and (2) giving Minkowski grids due to wave interference in Fig.3.

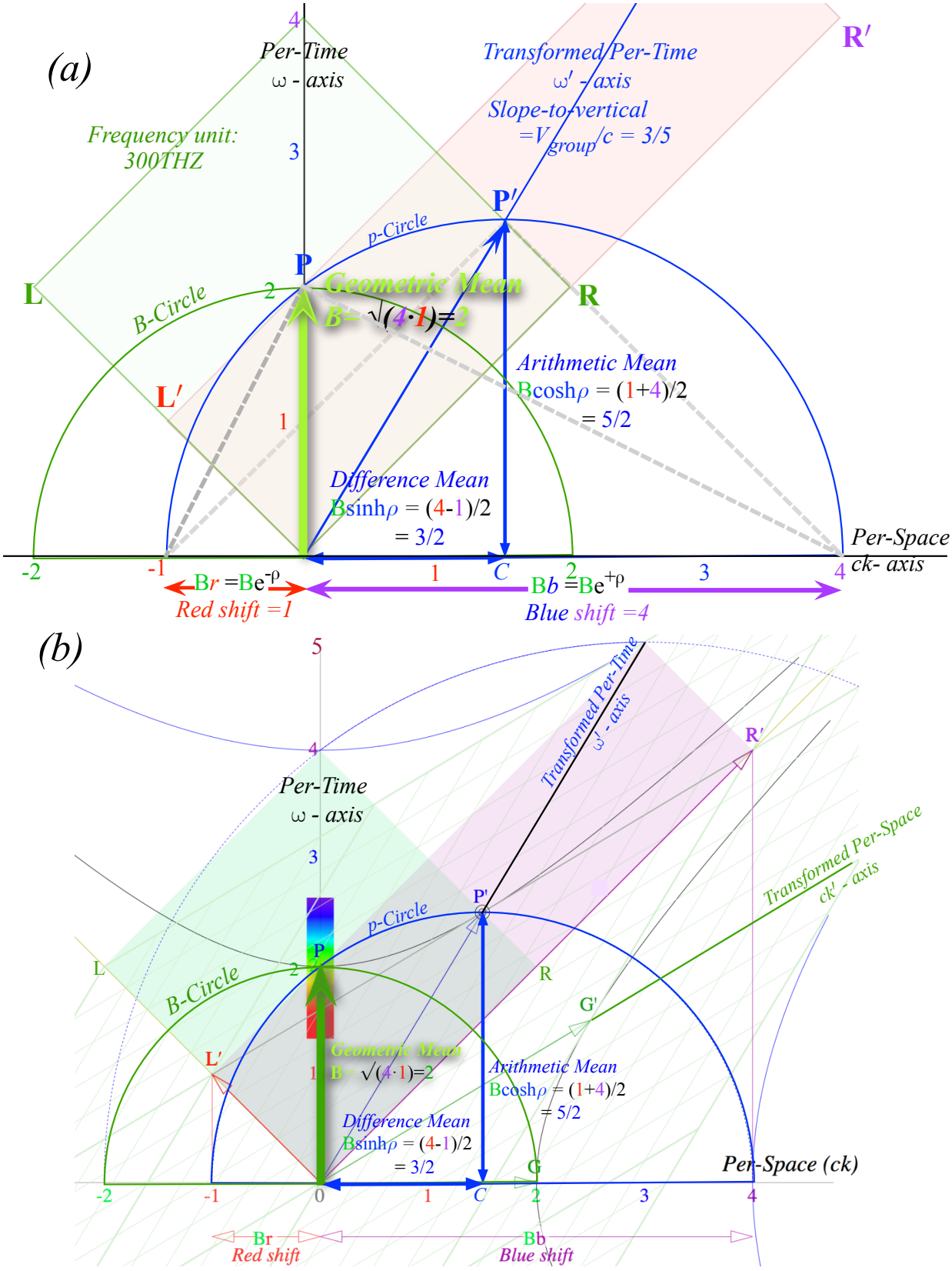

Fig. 5 (a)Thales-Euclid geometric and arithmetic means (b) Hyperbola construction step for circle radius **CP′**.

Web Simulation - RelaWavity: Thales-Euclid geometric relations of Per-space-time

Fig. 5 (c) Sum $\psi_{AB} = \psi_A + \psi_B$. (d) Sum of individual phasors. (e) Phasor *A* moves relative to *B* and vice-

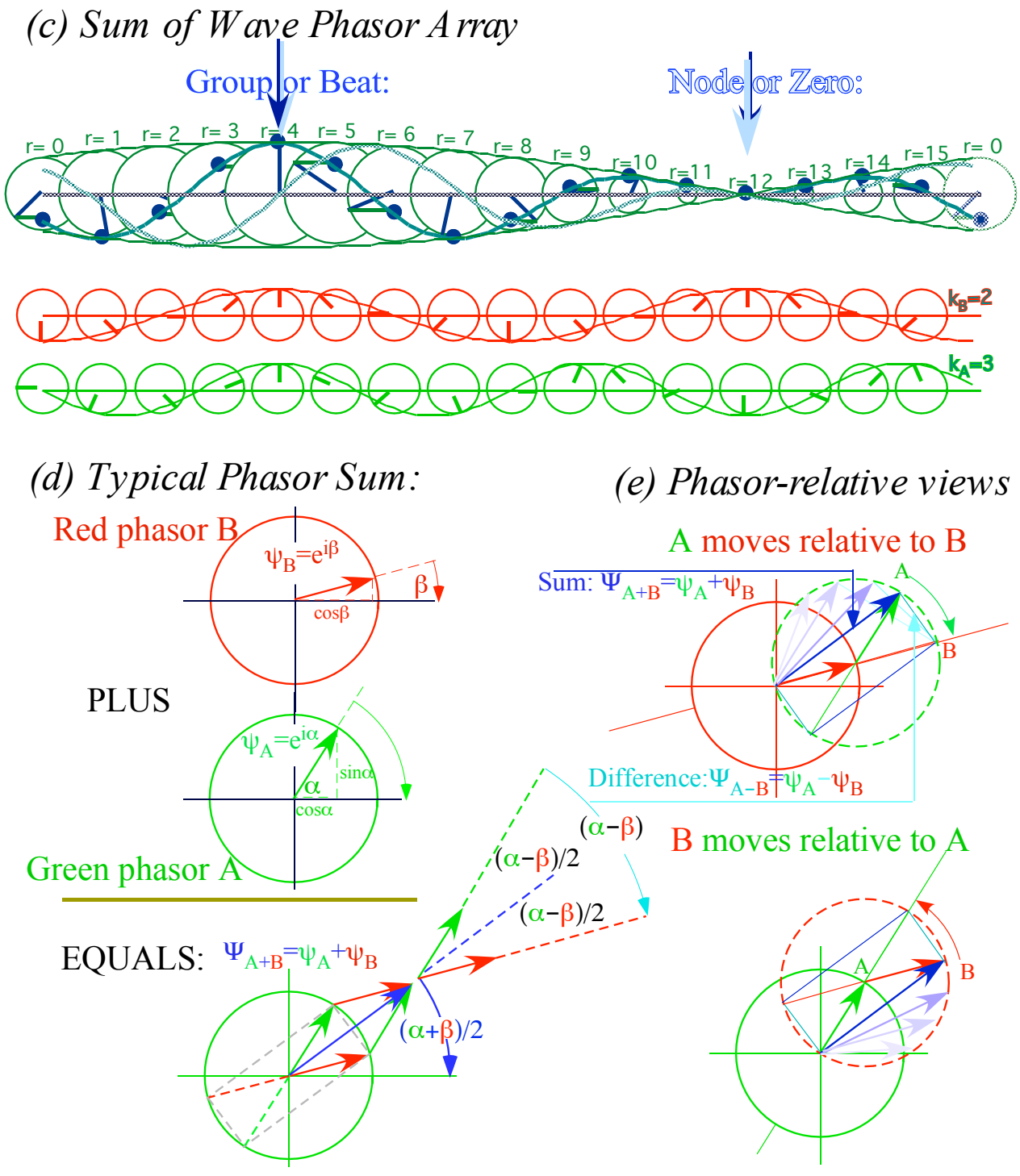

versa.

Pirelli Challenge Site animations: Phasor Addition, Phasor Description of Wave Interference

A novel review of trigonometry and some relawavity applications

Every scientific calculator has an SIN button and, as we tell our home-churched students, this is not such a bad thing. In fact it stands for Slope of INcline and (multiplied by 100) gives the percent of grade or ratio of altitude gained over road distance traveled along the freeway by their town. Next to SIN is a COS or COmplimentary Slope giving ratio of level distance over road distance. Fig. 6a is a plot of sine ($\sin\sigma=\frac{3}{5}$) and cosine ($\cos\sigma=\frac{4}{5}$) of angle $\angle\sigma=36.87°$ that makes 3:4:5 triangles. Angle in radians $\sigma=0.6435=\pi\frac{36.87°}{180°}$ is also total sector area for a unit ($B=1$) circle. (That is π for $\sigma=\pi$.) Fig. 6 use a non-standard convention to plot complimentary $\cos\sigma$ as a vertical projection while $\sin\sigma$ is horizontal. This is to match Minkowski plots like Fig. 4b where space x is plotted on horizontal axis and time t on the vertical axis. It is complimentary to a standard Newtonian plot of x (vertical) versus time (horizontal).

The result of pressing a calculator TAN button for angle $\angle\sigma=36.87°$ is the TANgent or $\tan\sigma=¾$ (the ratio $\tan\sigma=\frac{\sin\sigma}{\cos\sigma}$) labeling the hypotenuse of a smaller 3:4:5 triangle on top of Fig. 6a. That tangent line is also the altitude of the largest 3:4:5 triangle in Fig. 6a, and it encloses the upper σ-sector. The three circular functions $\sin\sigma$, $\cos\sigma$, and $\tan\sigma$ are sufficient for elementary physics but it helps to have three more that are inverses of the primary three. The secant ($\sec\sigma=\frac{1}{\cos\sigma}=\frac{5}{4}$), cosecant ($\csc\sigma=\frac{1}{\sin\sigma}=\frac{5}{3}$), and cotangent ($\cot\sigma=\frac{1}{\tan\sigma}=\frac{4}{3}$) as plotted in Fig. 6b to show *two* additional (and larger) 3:4:5 triangles.

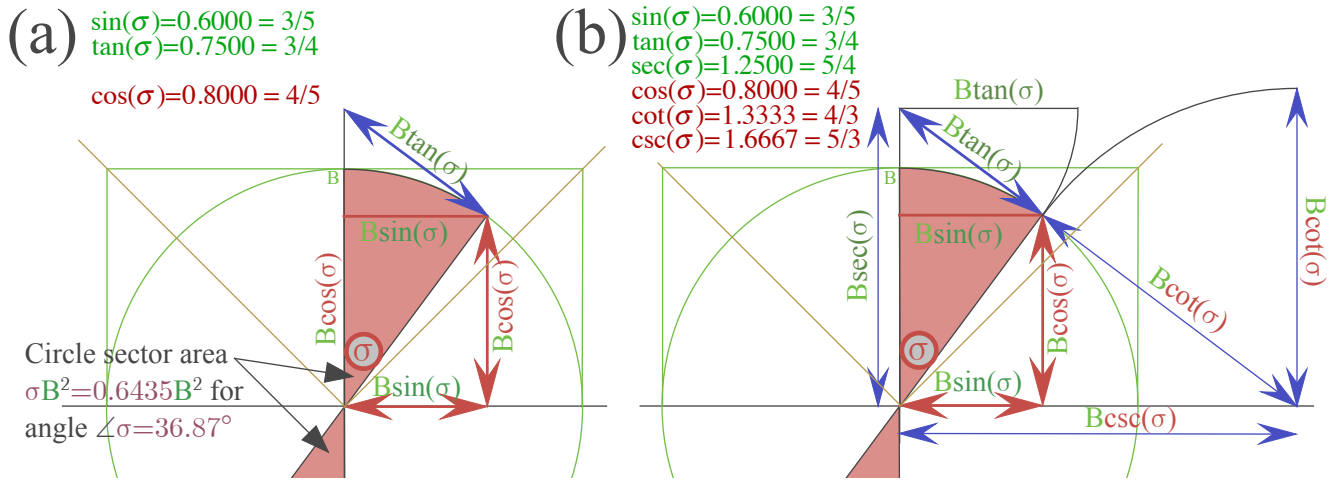

Fig. 6. Circular TRM's (a) Primary circular function triplet. (b) Full TRM sextet of circular functions.

Trigonometry suitable for SR and QM functional theory involves replacing six circular functions in Fig. 6b with six hyperbolic functions as shown in Fig. 7 and Fig. 8 that play similar roles in labeling coordinates, tangents, and their intercepts around an equilateral hyperbola. Each circular function (such as $\sin\sigma=\frac{3}{5}$) is like an "urban dweller" that has a "country cousin" (for $\sin\sigma=\frac{3}{5}=\tanh\rho=\frac{3}{5}$) with same numerical value ($\frac{3}{5}$ here) that is a function of hyperbolic sector area ($\rho=0.6931$ with angle $\measuredangle v=30.96°$ in this example) as listed on top of Fig. 7 and plotted nearby. For each country-urban pair there is a flipped pair (here: $\tan\sigma=\frac{3}{4}=\sinh\rho$) that shares a value ($\frac{3}{4}$ in that example) for the same hyper sector ($\rho=0.6931$ or angle $\measuredangle v=30.96°$) and corresponding circle sector ($\sigma=0.6435$ or angle $\angle\sigma=36.87°$). A circle-hyperbolic ("urban-country") pair $\sin\sigma=\frac{3}{5}=\tanh\rho$ and $\tan\sigma=\frac{3}{4}=\sinh\rho$ is listed on top left of Fig. 7 and plotted to the right below. (Fig.7 plots hyperbolic ρ-labels. Fig.6b plots circular σ-labels.)

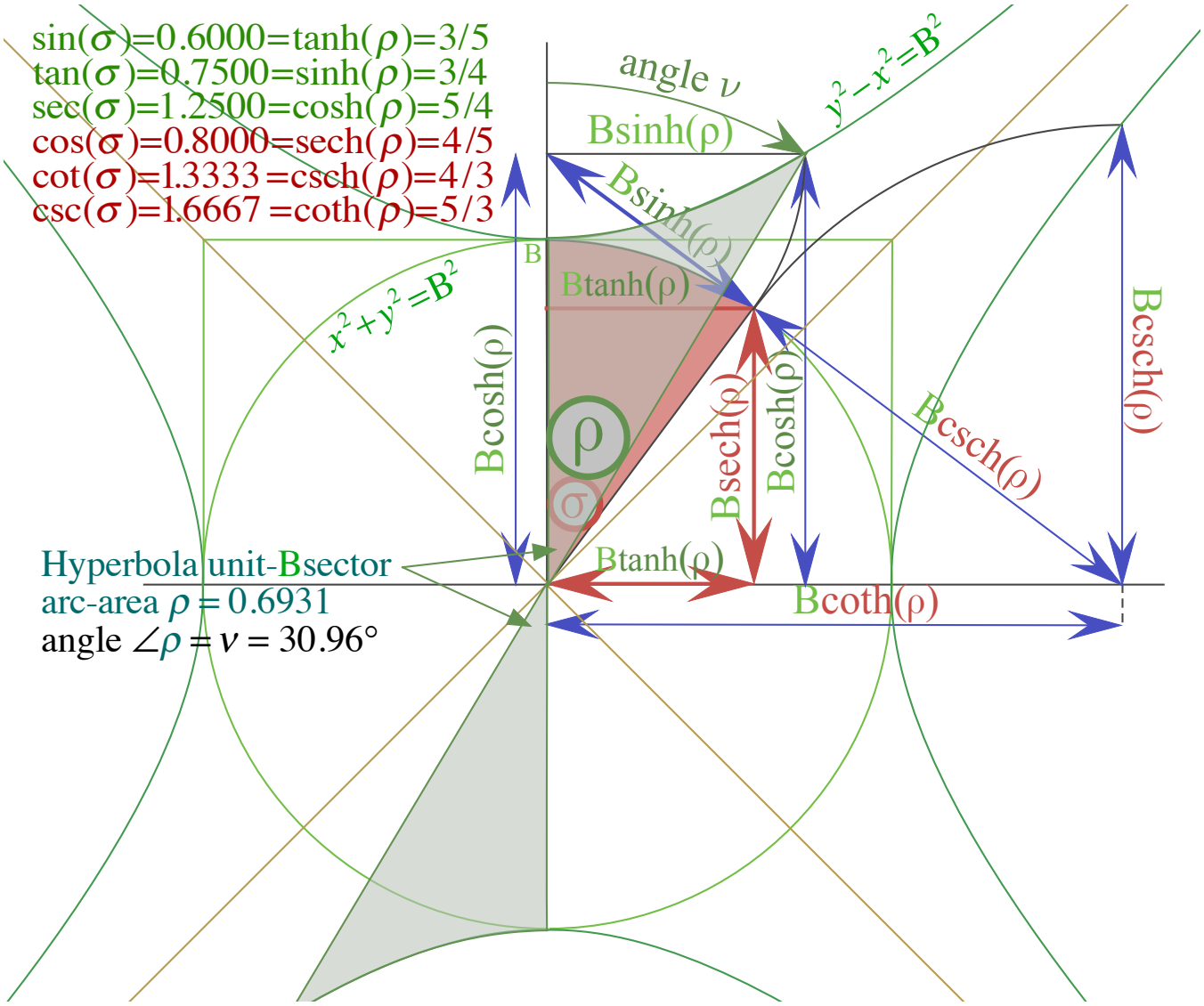

Total area ρ of paired sectors connecting opposite sides of a hyperbola is derived by an integral similar to one giving total sector area σ connecting sides of a circle.

Fig. 7 Labeling of Fig.3 coordinate geometry by hyperbolic functions of rapidity $\rho=\ln[v_{receiver}/v_{source}]$.
Web Sim - RelaWavity: Hyper-circular geometry w/hyperbolic labeling (Note: Web plot is reflected about x= y)

Relativity and quantum physics connects to this hyper-trigonometry through the hyper-parameter ρ or *rapidity* that is the logarithm of Doppler frequency ratio ($\rho=\ln[v_{receiver}/v_{source}]$) in Fig. 4 and Table 1. ρ is related by Eq.(3a) to the old-fashioned relativistic velocity parameter ($\beta\equiv\frac{u}{c}$) as follows.

$$\beta\equiv\tfrac{u}{c}=\tanh\rho=\tanh\left(\ln\frac{v_{receiver}}{v_{source}}\right) \tag{6a}$$

$$\beta\equiv\tfrac{u}{c}=\sin\sigma \tag{6b}$$

$$\beta\equiv\tfrac{u}{c}=\tan\nu \tag{6c}$$

Rapidity ρ is a *longitudinal* measure of group velocity along observer velocity **u**. An alternative speed parameter, namely *stellar aberration angle* σ in Fig.6, measures **k**-vectors *transverse* to observer velocity **u**. σ

appears in Fig. 8 and is physically defined in Fig. 9 below. A third speed parameter is angle v subtended by a ρ-sector in Fig.7 or Fig.8. It is the angle $\measuredangle_{\mathbf{P}}^{\mathbf{P}'}$ between rest ct (or x) and ρ-moving ct' (or x') axes in space-time.

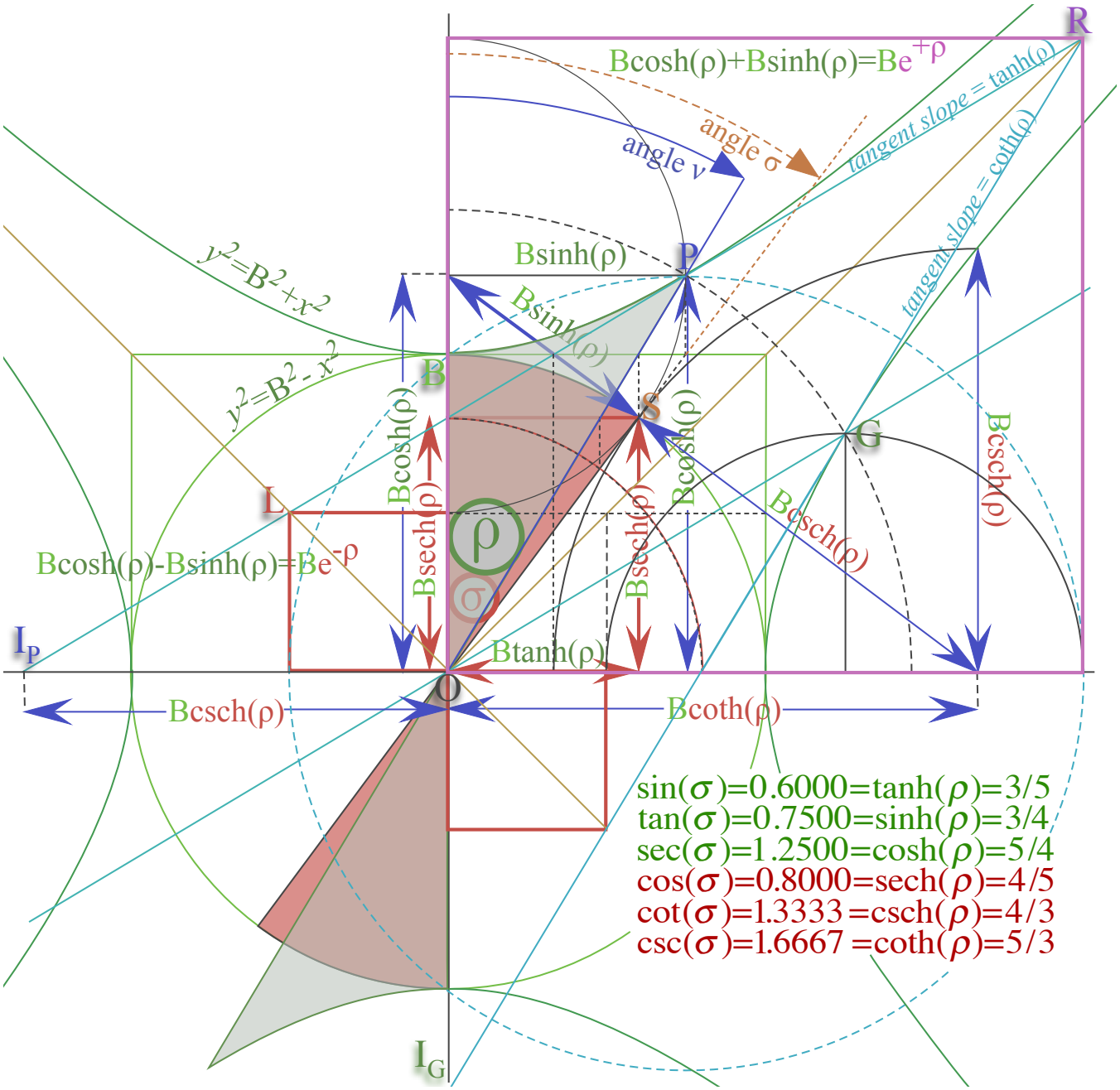

Fig. 8 Expanded ρ-labeling showing $e^{-\rho}$ vector (**P-G**)=**L**, $e^{+\rho}$ vector (**P+G**)=**R**, and Stellar vector **S** at angle σ.
UAF link to hyper-circular geometry with added detail

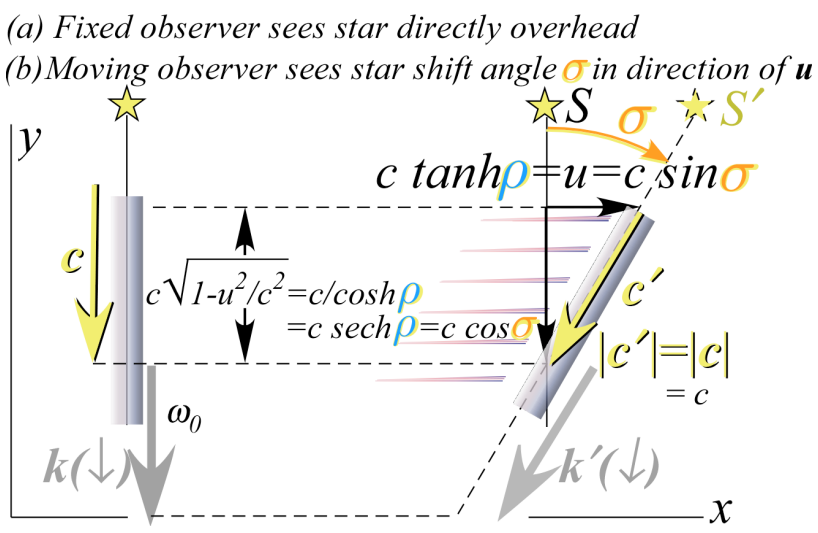

Fig. 9 Stellar aberration angle σ of light beam normal to direction of velocity **u**.

Lewis C. Epstein[1] developed a novel alternative to Minkowski-(x,ct)-plots that involves flipping proper-time definition $c^2\tau_A^2=c^2t'^2-x'^2$ as follows into a Cartesian Pythagorean relation $c^2\tau_A^2+x'^2=c^2t'^2$.

A Pythagorean geometry for space-proper-time or ($x,c\tau$)-plots is shown by Fig. 10. There it is imagined all things travel at light-speed c including a stationary object ($x'=0$) that "moves" parallel to the ($c\tau$)-axis. Moving object P is indicated by an vector (ct') that is inclined at aberration angle σ and also grows at rate c as given by $c^2\tau_A^2+x'^2=c^2t'^2$ with ($x'=u\cdot t'$). Fig. 10 animations relate ($x,c\tau$) to (x,ct).

Combining longitudinal rapidity ρ for hyperbolic geometry with transverse σ of circular geometry is useful and insightful. Applications to wave guide and cavity relawavity and quantum wave mechanics follow a use of ρ and σ relations developed in Fig. 7 and Fig. 8 and further in Fig. 11 below or later in Fig. 12.

At low group speed u ($u<<c$) the angles v, ρ, and σ in (3) converge to the old parameter $\beta=u/c$.

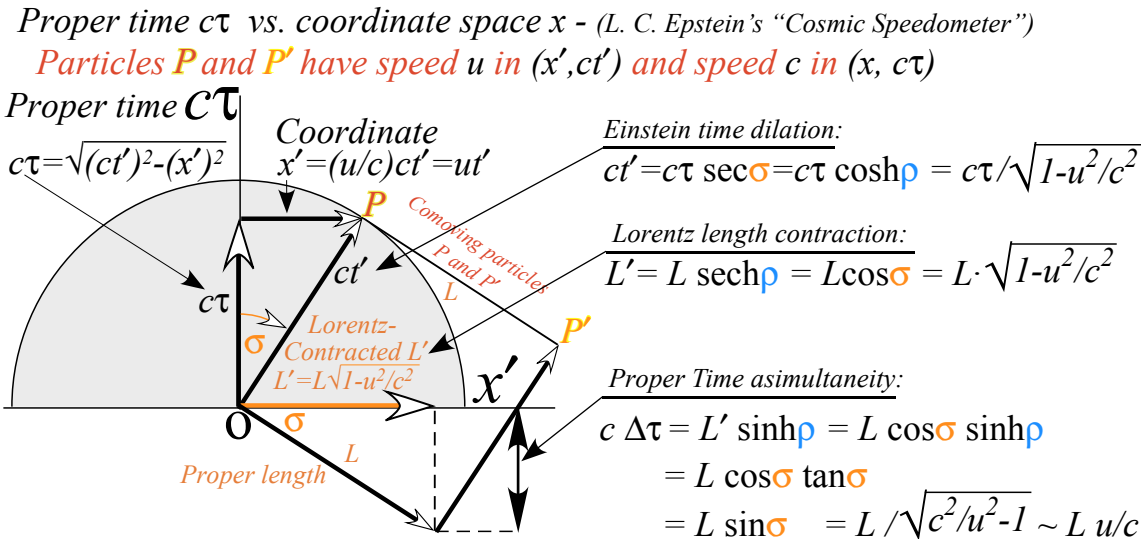

Fig. 10 Epstein space-proper-cτ geometry of relativistic effects in terms of ρ or σ.
UAF link to Epstein waves

[1] L. C. Epstein, *Relativity Visualized*. (Insight Press 1981) Transverse rotation provides an alternative view of relativity.

Fig.11 below combines the geometry of stellar aberration angle σ with a detailed rapidity ρ geometry of Fig.8 in a per-spacetime (υ,$c\kappa$)-plot of frequency ($\upsilon=\omega/2\pi$) versus wavenumber ($\kappa=k/2\pi$). The latter is rescaled to $c\kappa$ to give unit slope $\upsilon/c\kappa=1=\omega/ck$ for light cone line O**R** of the blue laser.

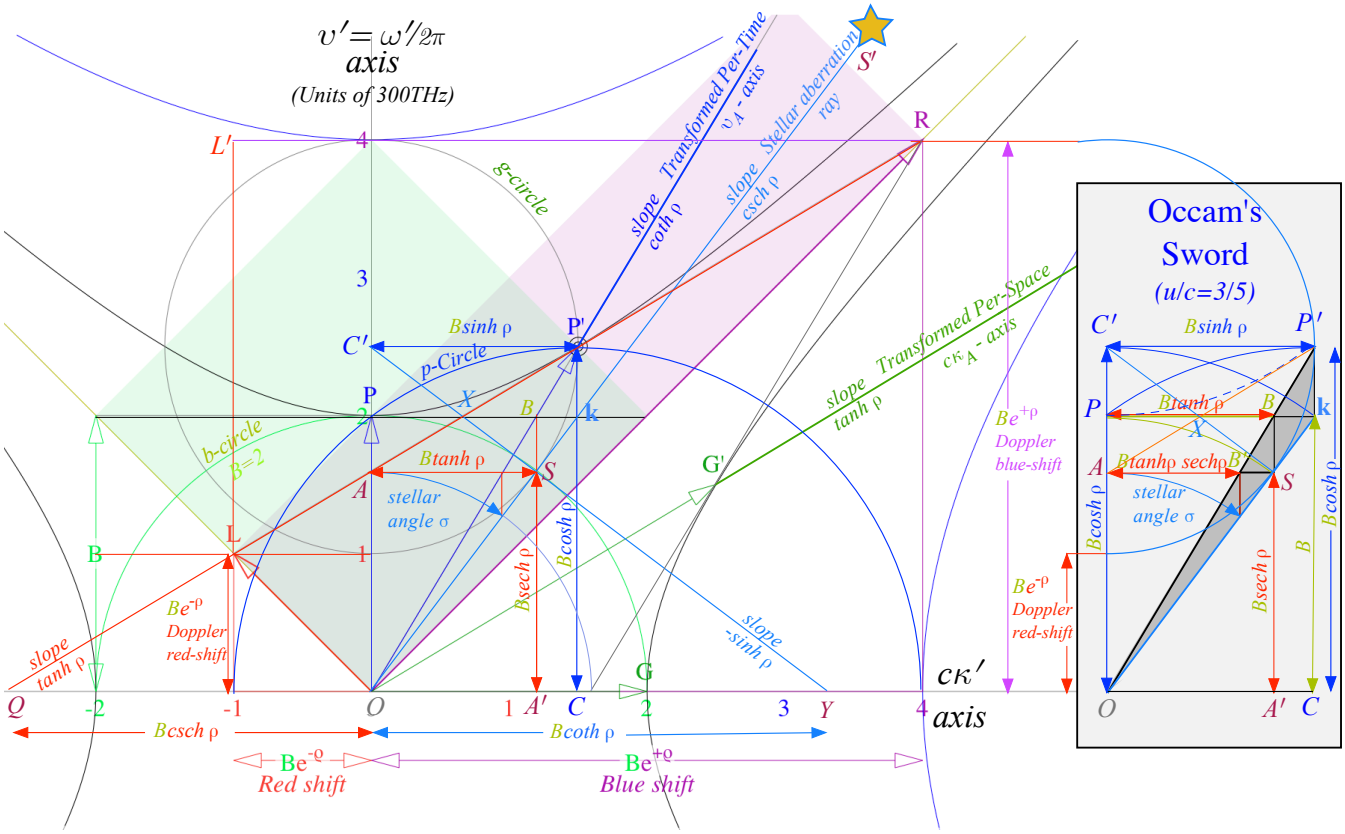

Fig. 11. (υ',$c\kappa'$)-view of rest frame (υ_A,$c\kappa_A$) tangent geometry and (inset) Occam-Sword pattern relating σ, ρ, and v angles.
UAF link to hyper-circular per-spacetime geometry

A pattern-recognition aid labeled *Occam's Sword* in Fig.11(inset) focuses on geometry of $(\sin \rightleftharpoons \tan)$ and $(\cos \rightleftharpoons \sec)$ columns in Table 1. The $(\cot \rightleftharpoons \csc)$ intercepts are outliers for low to moderate *u/c* values. The sword has a staircase whose steps belong to a $(\cosh\rho)^n$-geometric series: $(B\cosh\rho, B, B\sec\rho, ...)$. Extensions of the tangents have κ-axis $(\cot \rightleftharpoons \csc)$-intercepts on either side of the sword in Fig.11. The sword's lower **k**-edge defines wave vectors for waveguides and free-electron laser waves to aid analysis and visualization.

TE-Waveguide mode geometry

Consider a sum of plane waves with wave-vectors $\mathbf{k}^{(+)}=(k\sin\sigma,+k\cos\sigma)=(k_x,k_y)$ slanted up in Fig. 12a and $\mathbf{k}^{(-)}=(k\sin\sigma,-k\cos\sigma)=(k_x,k_y)$ slanted down, each at an angle $\pm\sigma$ relative to the *y*-axis in Fig 12.

$$E_z(\mathbf{r},t)=e^{i(\mathbf{k}^{(+)}\cdot\mathbf{r}-\omega\cdot t)}+e^{i(\mathbf{k}^{(-)}\cdot\mathbf{r}-\omega\cdot t)}=e^{i(k_x\cdot x-\omega\cdot t)}[e^{ik_y\cdot y}+e^{-ik_y\cdot y}] \qquad (7)$$

The result in *xy*-plane is a Transverse-Electric-(TE)-mode **E**-field with plane-normal *z*-component E_z that vanishes on metallic floor and ceiling ($y=\pm Y/2$) of the waveguide.

$$E_z(\mathbf{r},t)=e^{i(k\cdot x\sin\sigma-\omega\cdot t)}2\cos(ky\cos\sigma)\,|_{y=\frac{Y}{2}}=0 \quad \text{implies:} \quad k\frac{Y}{2}\cos\sigma=n\frac{\pi}{2} \qquad (8)$$

Fig.12 shows two cases of lowest ($n=1$) guide modes with Occam-sword geometry of Fig.11. Projection $Y\cos\sigma$ in Eq. (8) of floor-to-ceiling *Y* onto $\mathbf{k}^{(\pm)}$-vectors is shown by right triangles at guide ends to be $\frac{\pi}{k}=\frac{\lambda}{2}$, that is a half wave $\frac{\lambda}{2}$. Waveguide angle σ and dispersion function $\upsilon(\kappa)$ follows.

$$\upsilon = c\kappa = c\sqrt{\kappa_x^2+\kappa_y^2} = c\sqrt{\kappa_x^2+\kappa^2\cos^2\sigma} = \sqrt{c^2\kappa_x^2+(\frac{c}{2Y})^2} = \sqrt{c^2\kappa_x^2+\upsilon_A^2} \qquad (9)$$

Some insight into Fig.12 waves results if we note it is what you see if υ_A= 600THz 2-CW beams are directed *across* *x*-line of motion at angle σ to *y* and not *along* *x* as in Fig. 2. You may adjust your speed so that wave-number κ_x and angle σ drop to zero and frequency υ in (9) reduces to $\upsilon = \upsilon_A$. Such an *x*-flat ($\kappa_x = 0$) wave is a *cut-off-frequency* mode where $\upsilon_{CUTOFF} = \frac{c}{2Y} = \upsilon_A$ is the lower bound to the $\upsilon(\kappa_x)$ hyperbola that allows for waves entering a waveguide of width *Y*. Fig.12a mode is further above cut-off than one in Fig.12b.

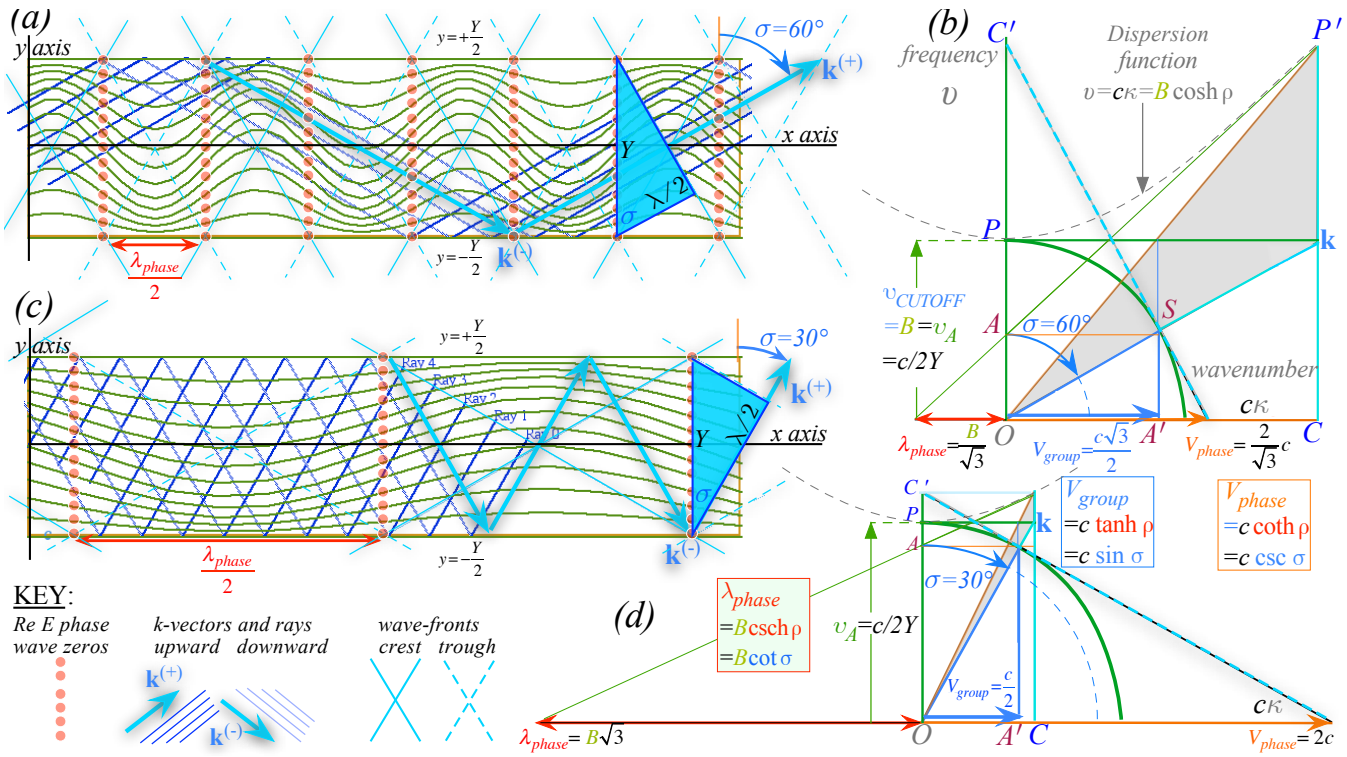

Fig. 12 TE-Waveguide and Occam sword geometry for stellar angle (a-b) σ = 60° and (c-d) σ = 30°.
UAF links to waveguide animation σ=60°. https://modphys.hosted.uark.edu/markup/GuideItWeb.html?scenario=230
link to σ=30°. https://modphys.hosted.uark.edu/markup/GuideItWeb.html?scenario=260

Relawavity derivation of basic quantum wave mechanics

During the 20th century, fundamental developments of quantum mechanics have relied on concepts from advanced classical mechanics of Lagrange, Hamilton, Legendre, Jacobi, and Poincare that were developed mostly in the preceding(19th) century. The latter contain a formidable web of formalism using ecclesiastical terms such as *canonical* that once implied higher levels of truthiness, but for modern physics students, that means not so much.

A simpler approach connects light wave geometry of Table 1 thru Fig.11 to 17th century mechanics of Galileo, Kepler, and Newton. This lets us derive quantum fundamentals for the 20th and 21st centuries while clarifying some of those 19th century classical concepts that are so often explained poorly or not at all.

2-CW geometry of Fig. 11 has hyperbolic coordinates of phase frequency $\upsilon_{phase}=B\cosh\rho$ and c-scaled wave number $c\kappa_{phase}=B\sinh\rho$ whose ratio is group velocity $V_{group}/c=u/c=\tanh\rho$. Each depends on rapidity ρ that approaches u/c for Galilean-Newtonian speeds $u \ll c$.

$$\begin{aligned} \upsilon_{phase} &= B\cosh\rho \approx B+\tfrac{1}{2}B\rho^2 \quad (\text{for } u \ll c) \\ c\kappa_{phase} &= B\sinh\rho \approx B\rho \quad (\text{for } u \ll c) \\ u/c &= \tanh\rho \approx \rho \quad (\text{for } u \ll c) \end{aligned} \tag{10}$$

Low speed κ_{phase} and υ_{phase} are functions of group velocity $u=c\rho$ or $u^2=c^2\rho^2$. Hyperbolic base coefficient B has frequency units ($1Hz=1s^{-1}$) of υ_{phase} or $c\kappa_{phase}$. Let B/c^2 multiply u^2 and u to get υ_{phase} and κ_{phase}.

$$\upsilon_{phase} \approx B+\tfrac{1}{2}[B/c^2]u^2 \quad \Leftarrow \text{for } (u \ll c) \Rightarrow \quad \kappa_{phase} \approx [B/c^2]u \tag{11}$$

From freshman physics we recall kinetic energy $KE=const.+\frac{1}{2}Mu^2$ and Galilean momentum $p=Mu$. One *Joule·s* scale factor $h=Mc^2/B$ gives υ_{phase} energy units and κ_{phase} momentum units. Such wave variables give classical KE and p formulas. But, an annoying (and large) constant Mc^2 is added to KE!

$$h\upsilon_{phase} \approx Mc^2+\frac{1}{2}Mu^2 \quad \Leftarrow \text{for } (u \ll c) \Rightarrow \quad h\kappa_{phase} \approx M\,u \tag{12}$$

One might ask, "Is this Mc^2 meaningful or just a lucky coincidence? Does an "empty" box of light have an Mc^2?"

Possible answers involve the base or bottom value $B=\upsilon_A$ of the frequency hyperbola. It is also every observer's bottom since that hyperbola appears the same for observers going *all* speeds low or *high*.

That h-scaled base coefficient $const.=hB=h\upsilon_A=Mc^2$ may be the most famous formula in physics. Here it is Einstein's rest-mass-energy equation. It is an add-on to Newton's kinetic energy $\frac{1}{2}Mu^2$ that is perhaps the *second* most famous physics formula, and the add-on does not contradict it since energy effects depend only on *difference* or *change* of energy that is unaffected since add-on constants cancel.

Finally, we replace approximate υ_{phase} and κ_{phase} in (12) by exact $\upsilon_{phase}=B\cosh\rho$ and $c\kappa_{phase}=B\sinh\rho$ for *all* ρ.

$$\begin{aligned} E = h\upsilon_{phase} &= Mc^2\cosh\rho \quad \Leftarrow \text{for } all\ \rho \Rightarrow \quad p = h\kappa_{phase} = Mc\sinh\rho \\ &= \frac{Mc^2}{\sqrt{1-u^2/c^2}} \quad \Leftarrow \text{for } |u|<c \Rightarrow \quad = \frac{Mu}{\sqrt{1-u^2/c^2}} \end{aligned} \tag{13}$$

An old-fashioned $\beta=u/c$ form of $\cosh\rho$ (Table 1) is the Einstein[2] 1905 total energy formula. Later in 1923, DeBroglie[3] gives wave momentum formula $p=\hbar k=h\kappa$ that has a $\beta=u/c$ form for $\sinh\rho$, too. Three lines above derive both ρ-forms from Table 1. This allows physics students to enjoy one-button-press calculator-recall as well as the geometric and algebraic elegance of relawavity efficiency.

Underlying (13) is considerable physics and mystery of "scale factor" h (or $\hbar \equiv h/2\pi$) the Planck constant $h=6.62607\cdot10^{-34}$ Joule·sec that appears in his cavity energy axiom $E_N=hN\upsilon$. Thus (13) gives just the lowest quantum level ($N=1$) of Planck's axiom[4]. (Modern form $E_N=\hbar N\omega$ has angular frequency $\omega=2\pi\upsilon$ and angular $\hbar=1.05\cdot10^{-34}Js$.) A quick-fix replaces h with hN, but underlying quantum oscillator theory of E&M cavity waves still needs discussion. (Introductory Fig.2-3 are, after all, semi-classical coherent quantum states.)

Apart from that, the only axioms needed to get (13) are Evenson's axiom (*All colors go c!*) and time reversal symmetry so red and blue Doppler shifts are reciprocal. These involve space, time, frequency and phase factors of plane light waves that are sufficient to develop the special relativity theory.

However, this phase approach ignores amplitude factor A of light wave $\psi = Ae^{i(\mathbf{k}\bullet\mathbf{r}-\omega t)}$. While phase factor $e^{i(\mathbf{k}\bullet\mathbf{r}-\omega t)}$ describes the *quality* aspects of the light, an amplitude factor A describes the *quantity* of light, or more to the point, an average number N of *quanta* or *photons* in a wave having the N factor of Planck's axiom. Raising N raises overall phase frequency $N\upsilon_{phase}$ and in proportion, both total energy $hN\upsilon_{phase}$ and total wave *quantum-mass* $M_N=(hN\upsilon_{phase})/c^2$. (This "light-weight" is tiny unless N is astronomical.)

Optical axioms leading to (13) shed some light on three of the most logically opaque concepts in physics, namely energy, momentum and mass by expressing them as phase frequency υ (inverse time τ) and wavenumber κ (inverse length λ). Perhaps, the terms *energy* and *momentum* could someday go the way of *phlogiston*!

What's the <u>matter</u> with energy?

Evenson axioms of optical dispersion and time symmetry imply a 2-CW light geometry that leads directly to exact mass-energy-momentum and frequency relations (13) with low-speed approximations (12). A light wave with rest mass and rest energy proportional to a proper invariant phase frequency.

$$\upsilon_{phase}=\upsilon_A=\upsilon'_A$$

This is effectively a quantum matter wave that, due to its phase frequency, acquires intrinsic rest mass.

$$M_{A_N}=Nh\upsilon_A/c^2 .$$

In so doing, concepts of mass or matter lose classical permanence and become fungible. We define three types of mass M_{rest}, M_{mom}, and M_{eff} distinguished by their dependence on rapidity ρ or velocity u. The first is $M_{rest} = M_{A_N}$. The other two approach M_{rest} at low $u \ll c$.

Einstein rest mass M_{A_N} is invariant to ρ. It labels a hyperbola with a bottom base level B_N.

$$E_N(\rho=0)=hB_N=M_{A_N}c^2 .$$

This is an invariant quantity for all observers. Each cavity or waveguide mode A has a base hyperbola (Recall Fig. 12b) under a ladder of hyperbolas each with its own tiny photon rest mass $M_{A_N}=NM_{A_0}$ and N-value $N=1,2,3,....$

---

[2] Albert Einstein "*Uber einen die Erzeugung und Verwandlung des Lichtes betreffenden heuristischen Gesichtspunkt.*" Annalen der Physik 17: 132-148 (1905). (Translation by A.B. Aarons and M.B. Peppard, Am. J. Phys. 33, 367(1965).)

[3] Louis de Broglie, Nature 112, 540 (1923); Annalen der Physik (10) 2 (1923).

[4] Max Planck "*Zur Theorie des Gesetzes der Energieverteilung im Normal-spectrum.*" Deutsche Physikalische Gesellschaft. Verhandlungen 2: 237-245 (1900).

$$E_N^2 = (hN\upsilon_A)^2 = \left(M_{A_N}c^2\right)^2 \cosh^2\rho = \left(M_{A_N}c^2\right)^2 (1+\sinh^2\rho)$$
$$= \left(M_{A_N}c^2\right)^2 + (cp_N)^2 \qquad (14)$$

Fig. 13a plots matter wave dispersion (13), the *(E, cp)*-hyperbola $E=\sqrt{(Mc^2)^2+(cp)^2}$ of Einstein-Planck. The inset Fig. 13b is a plot of approximation (12) for low p and $u \ll c$. A serious problem for that *Bohr*[5]*-Schrodinger*[6] *approximation* to quantum theory is that it gives a V_{group} greater than V_{phase}.

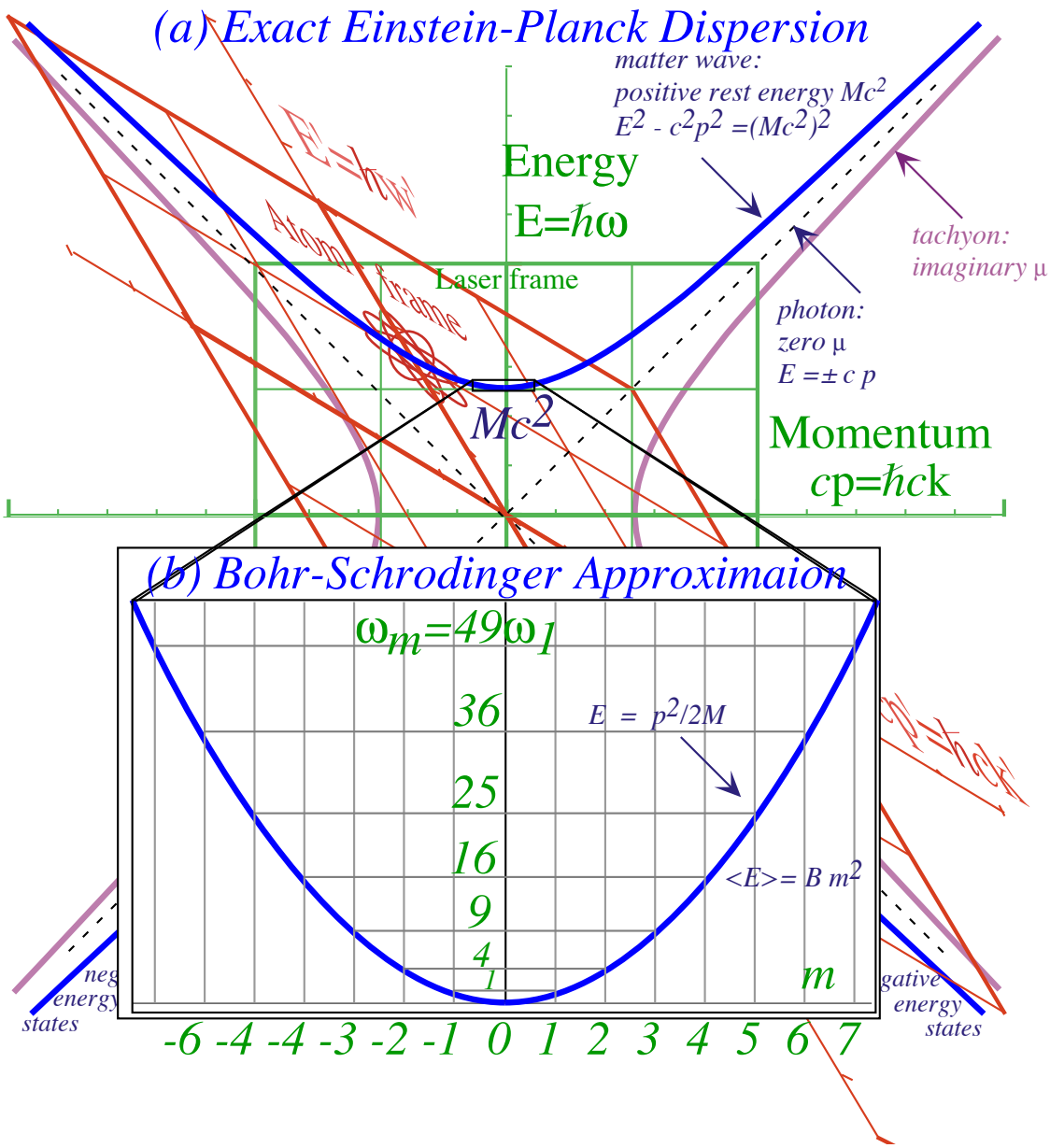

Fig. 13 (a) Einstein-Planck energy-momentum dispersion (b) Bohr-Schrodinger approximation

---

[5] N. Bohr, *Zeitschrift fur Physik*, 9, 1-2, (1922).

[6] E. Schrodinger, Annalen der Physik (4) 79 361 and 489 (1923); 80, 437 (1926); 81,109 (1926).Schrodinger's protests about prevailing quantum mechanical interpretations are well circulated. So far we have not located more solid references.

A second type of mass M_{mom} is *momentum-mass* defined by ratio *p/u* of $p=Mc\sinh\rho$, the relativistic momentum from (13) with group velocity $u=c\tanh\rho$ from (3a). M_{mom} satisfies Galileo's very old quasi-definition $p=M_{mom}u$, but now using the newly defined relativistic wave quantities *p* and *u*.

$$\frac{p}{u} \equiv M_{mom} = \frac{M_{rest}c}{u}\sinh\rho = M_{rest}\cosh\rho \xrightarrow[u\to c]{} M_{rest}e^{\rho}/2 \qquad (15)$$
$$= \frac{M_{rest}}{\sqrt{1-u^2/c^2}} \xrightarrow[u\ll c]{} M_{rest}$$

A third type of mass M_{eff} is *effective-mass* defined by ratio *dp/du* of *change* of momentum $p=Mc\sinh\rho$ from (13) with *change* of group velocity $du=c\,\mathrm{sech}^2\rho\,d\rho$. M_{eff} satisfies Newton's quite old definition $F=M_{eff}a$, but now using these relativistic wave quantities.

$$\frac{F}{a} \equiv M_{eff} \equiv \frac{dp}{du} = \frac{dp}{d\rho}\Big/\frac{du}{d\rho} = M_{rest}c\cosh\rho / c\,\mathrm{sech}^2\rho = M_{rest}\cosh^3\rho \qquad (16)$$

Another derivation of M_{eff} uses group velocity $V_{group}=\frac{d\upsilon}{d\kappa}=u$ as the independent variable.

$$\frac{F}{a} \equiv M_{eff} \equiv \frac{dp}{du} = \frac{h\,d\kappa}{dV_{group}} = h\Big/\frac{d}{d\kappa}\frac{d\upsilon}{d\kappa} = h\Big/\frac{d^2\upsilon}{d\kappa^2} \qquad (17)$$
$$= M_{rest}\Big/\left(1-u^2/c^2\right)^{3/2} \xrightarrow[u\ll c]{} M_{rest}$$

Group velocity and its tangent geometry is a crucial but hidden part of the matter wave theory. Physicists tend to commit to memory a derivative formula $\frac{d\upsilon}{d\kappa}=\frac{d\omega}{dk}$ for group velocity and forget $\frac{\Delta\upsilon}{\Delta\kappa}=\frac{\Delta\omega}{\Delta k}$ that is a finite-difference formula from which the former is derived. The former may give wrong results while the latter is *exact* for discrete frequency spectra wherein the former may be ill-defined. The wave Minkowski coordinate geometry starts with half-difference ratios to give V'_{group} in primary *u*-formulae (15) and (16).

$$V'_{group}/c = \frac{\Delta\upsilon}{c\Delta\kappa} = \frac{\upsilon_R-\upsilon_L}{\upsilon_R+\upsilon_L} = \frac{e^{\rho}-e^{-\rho}}{e^{\rho}+e^{-\rho}} = \tanh\rho \qquad (18)$$

What followed in Fig. 3 through Fig. 5 and Fig. 11 was based entirely upon the more reliable finite-difference definition $\frac{\Delta\upsilon}{\Delta\kappa}=\frac{\Delta\omega}{\Delta k}$ that gives slope exactly.

Nevertheless, Nature is kind to derivative definition $\frac{d\upsilon}{d\kappa}=\frac{d\omega}{dk}$ as seen in Fig.15. There hyperbolic tangent slope of line **RL** with altitude $\Delta\upsilon=\upsilon_R-\upsilon_L$ and base $\Delta\kappa=\kappa_R-\kappa_L$ has a finite-difference slope exactly equal to the derivative of the hyperbola at tangent point **P′** on phase velocity line **OP′**. Geometry of Doppler action (18) is at play. That slope $\frac{d\upsilon}{d\kappa}=\frac{d\omega}{dk}$ equals $V'_{group}=u$ and is the velocity. It is also related to the momentum/energy ratio $\frac{c\mathbf{p}}{E}=\frac{c\mathbf{k}}{\omega}=\frac{\mathbf{u}}{c}$ noted before.

$$V_{group} = u = \frac{\Delta\upsilon}{\Delta\kappa} = \frac{d\upsilon}{d\kappa} = \frac{d\omega}{dk} = \frac{dE}{dp} = \frac{c^2p}{E} \qquad (19)$$

As slope $\frac{d\upsilon}{d\kappa}=u$ of dispersion hyperbola $\upsilon(\kappa)$ affects velocity *u* and relations with momentum *p*, so does curvature $\frac{d^2\upsilon}{d\kappa^2}$ affect acceleration *a* and its relation to force *F* or momentum time rate of change $\frac{dp}{dt}$ in the effective-mass M_{eff} equations (16) and (17). One is inclined to regard M_{eff} as a quantum mechanical result since it is a product of Planck constant *h* with inverse $\frac{d^2\upsilon}{d\kappa^2}$, the approximate *Radius of Curvature RoC*$=1/\frac{d^2\upsilon}{d\kappa^2}$ of dispersion function $\upsilon(\kappa)$.

Relawavity geometry of Hamiltonian and Lagrangian functions

The 2-CW matter-wave in Fig. 3 has a rest frame with origin $x'=0$ and $k'=0=k_{phase}$ where the invariant phase function $\Phi = kx-\omega t = k'x'-\omega' t'$ reduces to $\Phi=0-\varpi\tau$, a product of proper or base frequency $B=\varpi=Mc^2/\hbar$. The *(x,t)*-differential of phase is reduced as well to a similar negative mass-frequency (ϖ)-term.

$$d\Phi = kdx-\omega dt = 0\cdot 0-\frac{Mc^2}{\hbar}d\tau \equiv -\varpi d\tau \tag{20}$$

A proper-time interval $d\tau$ dilates to ρ-moving frame time interval *dt* by Einstein dilation relations in Table 1.

$$dt=\frac{d\tau}{\sqrt{1-u^2/c^2}}=d\tau\cosh\rho \quad\Leftrightarrow\quad d\tau = dt\sqrt{1-u^2/c^2}=dt\,\mathrm{sech}\rho \tag{21}$$

One of the more interesting tales of modern physics is a first meeting[7] between Dirac[8] and the younger Richard Feynman[9]. Both had been working on aspects of quantum phase and classical Lagrangian mechanics. Dirac mused about some formulas in one of his papers that showed similarities between a Lagrangian function and quantum phase. Feynman said abruptly, "That's because the Lagrangian <u>is</u> quantum phase!" That was a fairly radical bit of insight for the time. It needs its geometry clarified.

Phase, action, and Lagrangian functions

Feynman's observation needs some adjustment for units since Lagrangian *L* has *Joule* units of energy while phase Φ is a dimensionless invariant. A quantity *S* called *Action* is quantum phase Φ scaled by Planck's angular constant $\hbar=\frac{h}{2\pi}=1.05\cdot 10^{-34}\,J\cdot s$ and is the following time integral of *L*.

$$S\equiv\hbar\Phi\equiv\int L\,dt \quad \text{where:} \quad \hbar\equiv\frac{h}{2\pi}=1.05\cdot 10^{-34}\,Joule\cdot Second \tag{22}$$

Differentials of action and phase (20) with time (21) combine to re-express *Ldt*.

$$dS\equiv Ldt=\hbar\,d\Phi=-Mc^2d\tau=-Mc^2\sqrt{1-u^2/c^2}\cdot dt=-Mc^2dt\,\mathrm{sech}\rho \tag{23}$$

From ρ-frame time derivative $dt/d\tau$ (20) arises the Lagrangian in terms of rapidity ρ or stellar angle σ.

$$L=-Mc^2\sqrt{1-u^2/c^2}=-Mc^2\mathrm{sech}\rho=-Mc^2\cos\sigma \tag{24}$$

Table 1 supplies identity $\mathrm{sech}\rho=\cos\sigma$ for *L* in (24) and $\tanh\rho=\sin\sigma$ for group velocity *u*.

$$u\equiv V_{group}=c\tanh\rho=c\sin\sigma \tag{25}$$

A classical convention has Lagrangian *L* be explicit function of velocity. This is consistent with the low-$\rho\cong\frac{u}{c}$ approximation to Lagrangian (24) that recovers the Newtonian $KE=\frac{1}{2}Mu^2$ term in (12).

$$L=-Mc^2\sqrt{1-u^2/c^2}\xrightarrow[u\ll c]{}-Mc^2+\tfrac{1}{2}Mu^2+\ldots \tag{26}$$

A following discussion of explicit functionality for Hamiltonian *H(p)* and Lagrangian *L(u)* involves the geometry of Legendre contact transformation depicted in Fig. 14 below.

---

[7] C. Sykes, *No Ordinary Genius: The Illustrated Richard Feynman* , W. Norton (1994) p. 84 (Meets Dirac in July 1964)

[8] P. A. M. Dirac, "Forms of Relativistic Dynamics" *Rev. Mod. Physics*, 21: 392 (1949).

[9] Feynman's Thesis: *A New approach to Quantum Theory*, Edited by Laurie M. Brown, World Scientific (2005) has edited copy of 1941 thesis and discussion of RPF *Space-time approach to non-relativistic quantum mechanics*, Rev. Mod. Phys. 20 (1948) pp. 367-387; and R. P. Feynman and A. R. Hibbs, *Quantum Mechanics and Path Integrals* (McGraw-Hill 1965)

Hamiltonian functions, Poincare invariants, and Legendre contact transformation

The invariant phase differential (40) with an $\hbar$-factor as in (43) is a key relation.

$$dS \equiv Ldt \equiv \hbar\, d\Phi = \hbar k dx - \hbar\omega dt \tag{27}$$

Energy $E=h\upsilon_{phase}=\hbar\omega=H$ and momentum $p=h\kappa_{phase}=\hbar k$ from (33) for *N=1* are used.

$$dS \equiv Ldt \equiv \hbar\, d\Phi = p\,dx - Hdt \quad \Rightarrow \quad L = p\frac{dx}{dt} - H = p\dot{x} - H \tag{28}$$

Here energy *E* is identified with Hamiltonian function *H*. Results include the classical *Poincare differential invariant* $Ldt=pdx-Hdt$ and the *Legendre transform* $L=pu-H$ between Lagrangian *L* and Hamiltonian *H*. Remarkably, it shows L/Mc^2 is the negative reciprocal of H/Mc^2.

$$H = \hbar\omega = Mc^2\cosh\rho = Mc^2\sec\sigma = \frac{Mc^2}{\sqrt{1-u^2/c^2}} \tag{29a}$$

$$L = \hbar\dot{\Phi} = -Mc^2\,\mathrm{sech}\rho = -Mc^2\cos\sigma = -Mc^2\sqrt{1-u^2/c^2} \tag{29b}$$

Except for a (-)sign, *H* and *L* are co-inverse (cos,sec)-cousin functions (mid-columns of Table 1 or 2). So are Einstein *t*-dilation and Lorentz *x*-contraction, respectively. *H* is explicit function of momentum *p* and *L* is explicit function of velocity *u*. So are *u* and *p* a *1st cousin* (sin,tan) pair in Table 1 or 2.

$$cp = \hbar ck = Mc^2\sinh\rho = Mc^2\tan\sigma = \frac{Mcu}{\sqrt{1-u^2/c^2}} \tag{30a}$$

$$u \equiv V_{group} = c\tanh\rho = c\sin\sigma \tag{30b}$$

Legendre contact transformation $H(cp)=pu-L=cpu/c-L$ uses slope u/c and intercept $-L$ of tangent line **LPR** contacting *H*-hyperbola in Fig. 14 at **P** and intercepting E-axis at point $-L(u)$ of Lagrangian. Inverse Legendre contact transformation $L(u)=pu-H$ uses slope *p* and intercept *H* of stellar tangent line *H***S** contacting the *L*-circle in Fig. 14 while intercepting *E*-axis at the height *H(p)* of the Hamiltonian phase point **P**.

Tangent contact transformation is a concept based upon wave properties and goes back to the Huygens and Hamilton principles discussed below. The basics of this lie in construction of space-time *(x,ct)* wave-grids given frequency-**k**-vectors $(\upsilon,c\kappa)$ like **P′** and **G′** in Fig. 4 or Fig. 11. Each **P′** or **G′** coordinate pair $(\upsilon,c\kappa)$ determines lines with speed υ/κ and *t*-intercept spacing $\tau = 1/\upsilon$ on *ct*-axis while *x*-intercept spacing is $\lambda=1/\kappa$ on *x*-axis. These phase and group grid lines make Minkowski zero-line coordinates.

This geometry applies as well to energy-momentum $(E,cp)=h(\upsilon,c\kappa)=\hbar(\omega,ck)$ spaces. Functional dependence of wave grid spacing and slopes determines classical variables, equations of motion, as well as functional *non*-dependence. For example, Lagrangian *L* is an explicit function of velocity *u* but *not* momentum *p*, that is, $\frac{\partial L}{\partial p}=0$. Hamiltonian *H* is explicit function of momentum *p* but *not* velocity *u*, that is, $\frac{\partial H}{\partial u}=0$. Such *0th*-equations combined with $L=pu-H$ give *1st*-Hamilton and *1st*-Lagrange equations.

$$0 = \frac{\partial L}{\partial p} = \frac{\partial}{\partial p}(pu-H) \Rightarrow u = \frac{\partial H}{\partial p}\left(\begin{smallmatrix}\text{Hamilton's}\\ 1^{st}\text{ equation}\end{smallmatrix}\right) \tag{31a}$$

$$0 = \frac{\partial H}{\partial u} = \frac{\partial}{\partial u}(pu-L) \Rightarrow p = \frac{\partial L}{\partial u}\left(\begin{smallmatrix}\text{Lagrange}\\ 1^{st}\text{ equation}\end{smallmatrix}\right) \tag{31b}$$

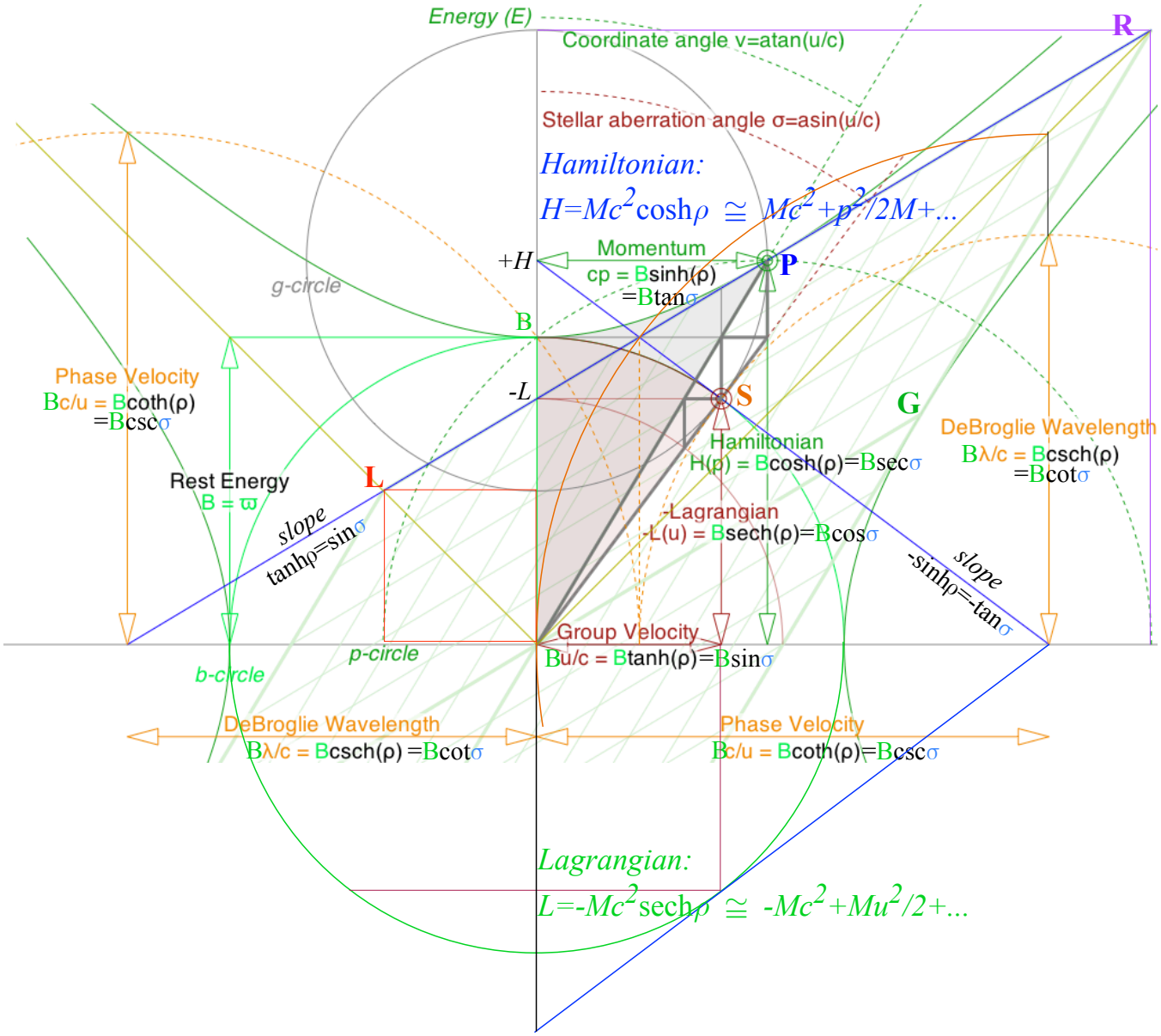

Fig. 14 Geometric elements of positive-energy relativistic quantum mechanics.
Relativistic trig map: https://modphys.hosted.uark.edu/markup/RelaWavityWeb.html?plotType=4,8

Hamilton-Jacobi quantization

Invariant phase Φ or action *S* differential (26) and (27) are integrable under certain conditions.

$$dS \equiv Ldt \equiv \hbar\, d\Phi = pdx - Hdt = \hbar k dx - \hbar\omega dt \tag{32}$$

That is each coefficient of a differential term *dq* in *dS* must be a corresponding partial derivative $\frac{\partial S}{\partial q}$.

$$\frac{\partial S}{\partial x} = p, \qquad \frac{\partial S}{\partial t} = -H. \tag{33}$$

These are known as *Hamilton-Jacobi equations* for the phase action function *S*. Classical *HJ*-action theory was intended to analyze families of trajectories (PW or particle paths). Dirac and Feynman related this to matter-wave mechanics (CW phase paths) by proposing approximate semi-classical wavefunction Ψ based on Lagrangian action $S=\hbar\Phi$ in its phase.

$$\Psi \approx e^{i\Phi} = e^{iS/\hbar} = e^{i\int L\,dt/\hbar} \tag{34}$$

Approximation symbol (≈) indicates that phase but not amplitude is expected to vary here. The *HJ* form $\frac{\partial S}{\partial x}=p$ turns x-derivative of Ψ into standard quantum **p**-operator form $\mathbf{p}=\frac{\hbar}{i}\frac{\partial}{\partial x}$.

$$\frac{\partial}{\partial x}\Psi \approx \frac{i}{\hbar}\frac{\partial S}{\partial x}e^{iS/\hbar} = \frac{i}{\hbar}p\Psi \qquad \Rightarrow \qquad \frac{\hbar}{i}\frac{\partial}{\partial x}\Psi = \mathbf{p}\Psi \tag{35a}$$

The *HJ* form $\frac{\partial S}{\partial t}=-H$ turns t-derivative of Ψ similarly into Hamiltonian operator $\mathbf{H}=\hbar i\frac{\partial}{\partial t}$.

$$\frac{\partial}{\partial t}\Psi \approx \frac{i}{\hbar}\frac{\partial S}{\partial t}e^{iS/\hbar} = -\frac{i}{\hbar}H\Psi \qquad \Rightarrow \qquad i\hbar\frac{\partial}{\partial t}\Psi = \mathbf{H}\Psi \tag{35b}$$

Action integral $S=\int L dt$ is to be minimized. Feynman''s interpretation of this is depicted in Fig. 15. Any mass M appears to fly so that its phase proper time τ is maximized. Proper mass-energy frequency $\varpi = Mc^2/\hbar$ is constant for a mass M. Minimizing $-\varpi\tau$ is thus the same as maximizing $+\tau$. Clocks near light cone tick slowly compared ones near max-τ on the natural true path. Those on light cone do not tick at all!

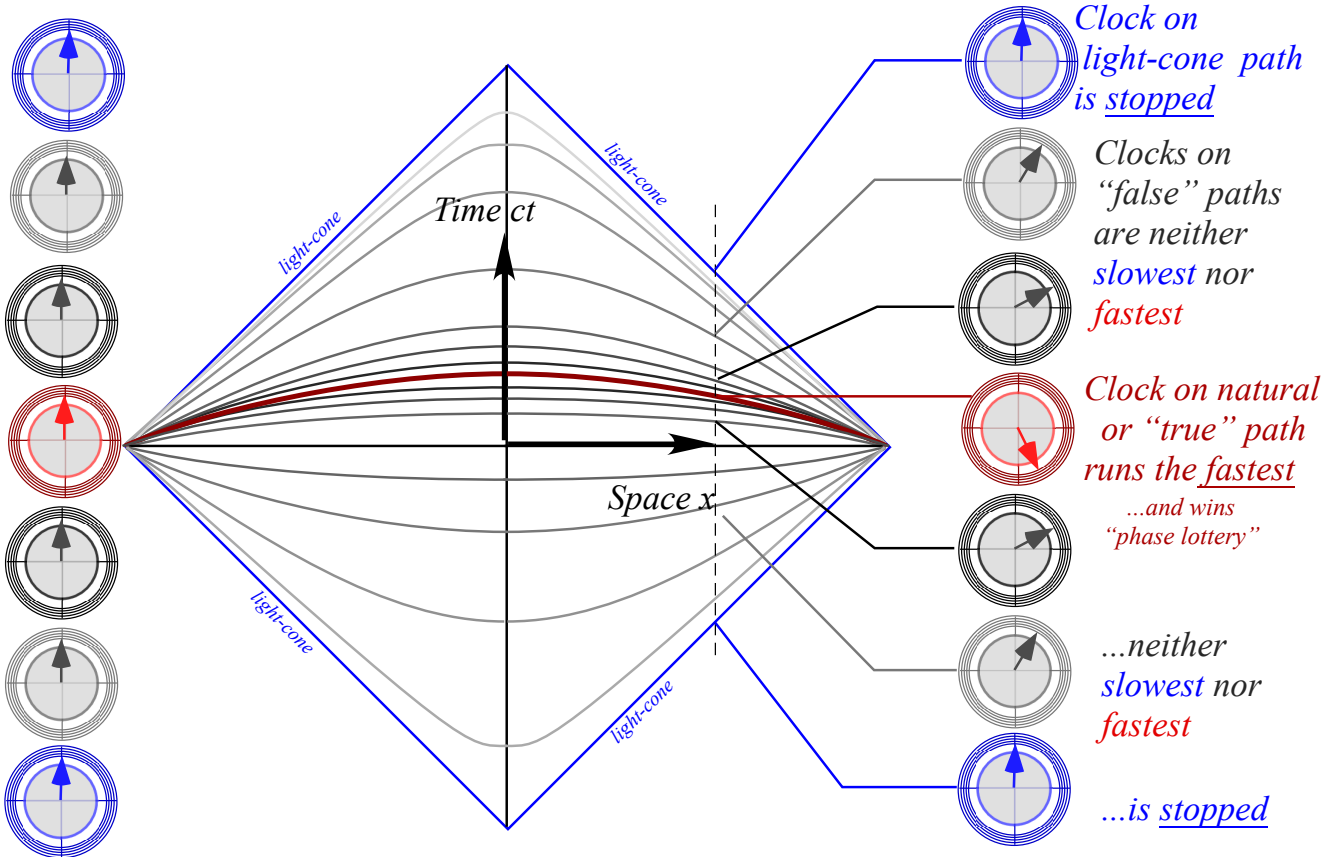

Fig. 15 Feynman's flying wave clock contest winner has the greatest advance of time by following the 'true' classical path.

One may explain how a flying mass finds and follows its max-τ path by imagining it is first a wave that could spread Huygen's wavelets out over many paths. But, an interference of Huygen wavelets favors stationary and extreme phase. This quickly builds constructive interference in the stationary phase regions where the the fastest possible clock path lies. Nearby paths contain a continuum of non-extreme or non-stationary wavelet phase that interfere *de*structively to crush wave amplitude off the well-beaten max-τ path as sketched in Fig. 16.

The very "best" are so-called stationary-phase rays that are extremes in phase and thereby satisfy Hamilton's Least-Action Principle requiring that $S=\int L dt$ is minimum for "true" classical trajectories. This in turn enforces Poincare invariance by eliminating, by de-phasing, any "false" or non-classical paths because they do not

have an invariant (and thereby stationary) phase. Thus “bad” rays” cancel each other in a cacophonous mish-mash of mismatched phases.

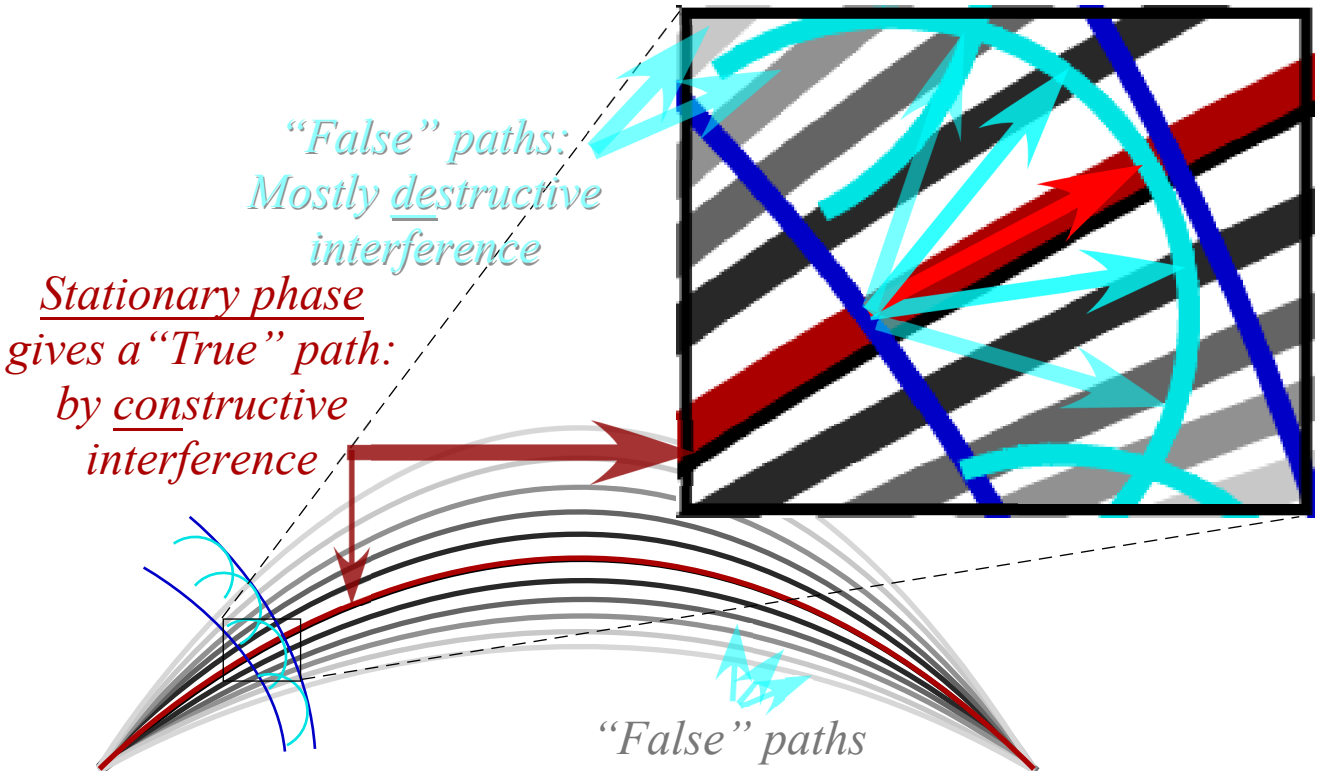

Fig. 16 Quantum waves interfere constructively on “True” path but mostly cancel elsewhere.

Each Huygen wavelet in Fig. 16 is tangent to the next wavefront being produced. That contact point is precisely on a ray or true classical trajectory path of minimum action and on the resulting “best” wavefront. Time evolution from any wavefront to the next is thus a contact transformation between two wavefronts described by this geometry of Huygens Principle.

Thus a Newtonian clockwork-world appears to be the perennial cosmic gambling-house winner in a kind of wave dynamical lottery on an underlying wave fabric. Einstein''s God may not play dice[10], but some persistently wavelike entities seem to be gaming at enormous $Mc^2/\hbar$ -rates down in the cellar! And in so doing, geometric order is created out of chaos.

[10] A. Einstein, *"I shall never believe that god plays dice with the universe"* Albert Einstein Archives, The Jewish National & University Library, The Hebrew University of Jerusalem (www.albert-einstein.org), Einstein Archives Online, Volume 15, #294, Letter to Cornelius Lanczos, March 21, 1942,http://www.alberteinstein.info/db/ViewDetails.do?DocumentID=30893.

Summary of relevant relativity tables (Identical entries but very different physics)

Relawavity space-time variable Table 2a

group	$b_{RED}^{Doppler}$	$\frac{V_{group}}{c}$	$\frac{\upsilon_{group}}{\upsilon_A}$	$\frac{\lambda_{group}}{\lambda_A}$	$\frac{\kappa_{group}}{\kappa_A}$	$\frac{\tau_{group}}{\tau_A}$	$\frac{V_{phase}}{c}$	$b_{BLUE}^{Doppler}$
phase	$\frac{1}{b_{BLUE}^{Doppler}}$	$\frac{c}{V_{phase}}$	$\frac{\kappa_{phase}}{\kappa_A}$	$\frac{\tau_{phase}}{\tau_A}$	$\frac{\upsilon_{phase}}{\upsilon_A}$	$\frac{\lambda_{phase}}{\lambda_A}$	$\frac{c}{V_{group}}$	$\frac{1}{b_{RED}^{Doppler}}$
rapidity ρ	$e^{-\rho}$	$\tanh\rho$	$\sinh\rho$	$\operatorname{sech}\rho$	$\cosh\rho$	$\operatorname{csch}\rho$	$\coth\rho$	$e^{+\rho}$
stellar $\forall$ *angle* σ	$1/e^{+\rho}$	$\sin\sigma$	$\tan\sigma$	$\cos\sigma$	$\sec\sigma$	$\cot\sigma$	$\csc\sigma$	$1/e^{-\rho}$
$\beta\equiv\frac{u}{c}$	$\sqrt{\frac{1-\beta}{1+\beta}}$	$\frac{\beta}{1}$	$\frac{1}{\sqrt{\beta^{-2}-1}}$	$\frac{\sqrt{1-\beta^2}}{1}$	$\frac{1}{\sqrt{1-\beta^2}}$	$\frac{\sqrt{\beta^{-2}-1}}{1}$	$\frac{1}{\beta}$	$\sqrt{\frac{1+\beta}{1-\beta}}$
value for β=3/5	$\frac{1}{2}$= 0.5	$\frac{3}{5}$=0.6	$\frac{3}{4}$=0.75	$\frac{4}{5}$=0.80	$\frac{5}{4}$=1.25	$\frac{4}{3}$=1.33	$\frac{5}{3}$=1.67	$\frac{2}{1}$=2.0
effects	$b_{RED}^{Doppler}$	V_{group}	*past-future asymmetry* (*off-diagonal Lorentz-transform*)	*x-contraction* (*Lorentz*) τ_{phase}*-contraction*	*t-dilation* (*Einstein*) υ_{phase}*-dilation* (*on-diagonal Lorentz-transform*)	*inverse asymmetry*	V_{phase}	$b_{BLUE}^{Doppler}$

Relawavity per-space-time (quantum mechanical) variable Table 2b

group	$b_{RED}^{Doppler}$	$\frac{V_{group}}{c}$	$\frac{\upsilon_{group}}{\upsilon_A}$	$\frac{\lambda_{group}}{\lambda_A}$	$\frac{\kappa_{group}}{\kappa_A}$	$\frac{\tau_{group}}{\tau_A}$	$\frac{V_{phase}}{c}$	$b_{BLUE}^{Doppler}$
phase	$\frac{1}{b_{BLUE}^{Doppler}}$	$\frac{c}{V_{phase}}$	$\frac{\kappa_{phase}}{\kappa_A}$	$\frac{\tau_{phase}}{\tau_A}$	$\frac{\upsilon_{phase}}{\upsilon_A}$	$\frac{\lambda_{phase}}{\lambda_A}$	$\frac{c}{V_{group}}$	$\frac{1}{b_{RED}^{Doppler}}$
rapidity ρ	$e^{-\rho}$	$\tanh\rho$	$\sinh\rho$	$\operatorname{sech}\rho$	$\cosh\rho$	$\operatorname{csch}\rho$	$\coth\rho$	$e^{+\rho}$
stellar $\forall$ *angle* σ	$1/e^{+\rho}$	$\sin\sigma$	$\tan\sigma$	$\cos\sigma$	$\sec\sigma$	$\cot\sigma$	$\csc\sigma$	$1/e^{-\rho}$
$\beta\equiv\frac{u}{c}$	$\sqrt{\frac{1-\beta}{1+\beta}}$	$\frac{\beta}{1}$	$\frac{\beta}{\sqrt{1-\beta^2}}$	$\frac{\sqrt{1-\beta^2}}{1}$	$\frac{1}{\sqrt{1-\beta^2}}$	$\frac{\sqrt{1-\beta^2}}{\beta}$	$\frac{1}{\beta}$	$\sqrt{\frac{1+\beta}{1-\beta}}$
value for β=3/5	$\frac{1}{2}$= 0.5	$\frac{3}{5}$=0.6	$\frac{3}{4}$=0.75	$\frac{4}{5}$=0.80	$\frac{5}{4}$=1.25	$\frac{4}{3}$=1.33	$\frac{5}{3}$=1.67	$\frac{2}{1}$=2.0
functions		$V_{group}=c\tanh\rho$	*momentum* $cp=Mc^2\sinh\rho$	*-Lagrangian* $L=-Mc^2\operatorname{sech}\rho$	*Hamiltonian* $H=Mc^2\cosh\rho$	*DeBroglie* $\lambda=\alpha\operatorname{csch}\rho$	$V_{phase}=c\coth\rho$	

Occam Sword geometry in (k_x,k_y) *and* (x,y)

A remarkable feature of relawavity geometry is that it appears to transcend 2D space-time *(x,ct)* or per-space-time (ck_x,ω). It applies as well to per-space-per-space (k_x,k_y) and plain old space-space *(x,y)*. Some examples are below.

Uniform circular arrays of **k**-vectors undergo relativistic variation of stellar (**k**-vector) aberration and Doppler frequency shifts when observed from a frame moving along the *x*-axis as shown in Fig. 17. Their k_y components do not vary with ρ. The tip of the **k**-vector (lower edge of the Occam Sword) grows along an *x*-parallel line while the **P′**-vector (upper edge) rises with its *x*-component identical to that of **k** as stellar angle σ of **k** grows.

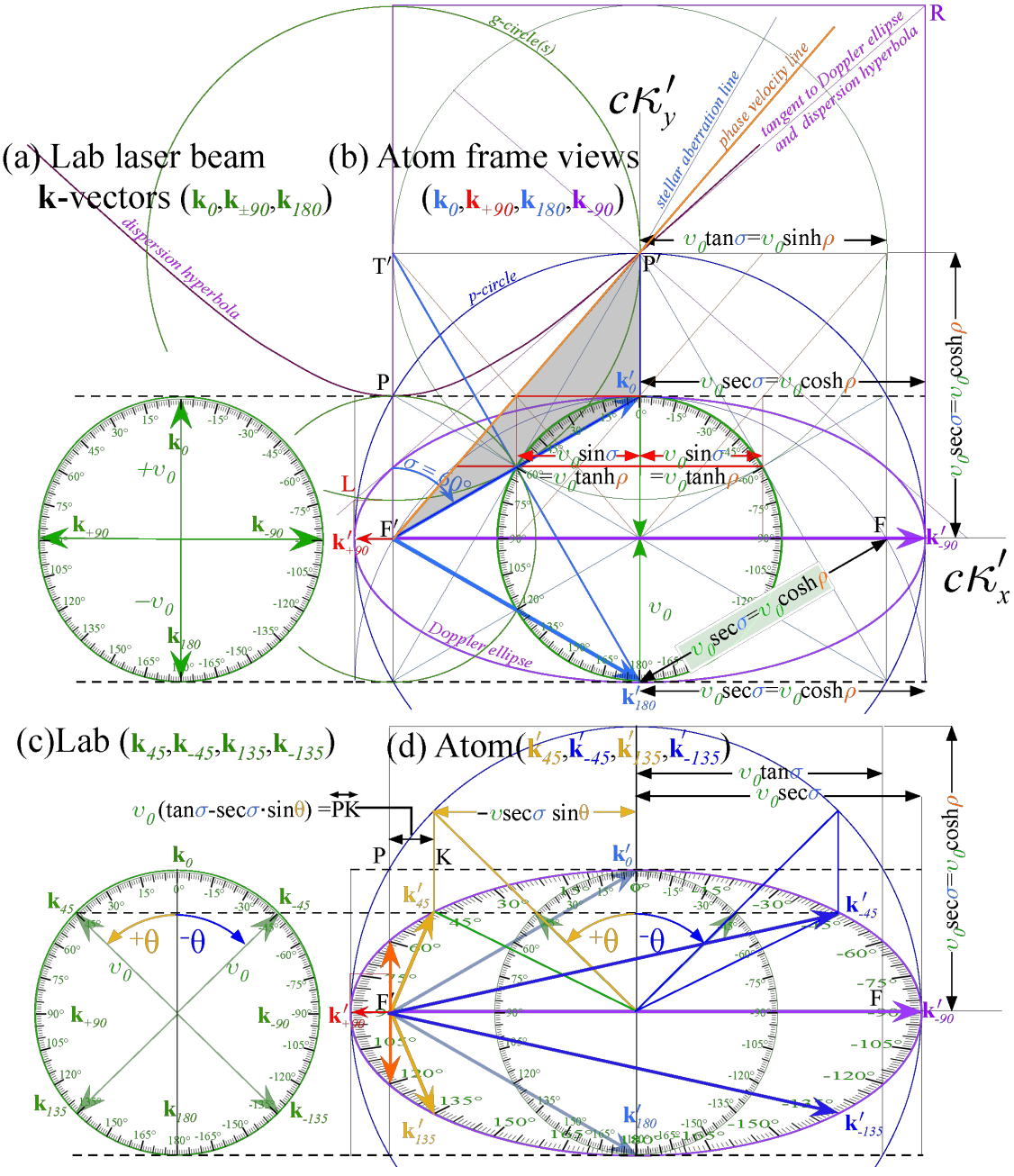

Fig. 17. 2D-array of 8 **k**-vectors on circular protractor become elliptical array around focus of elliptic protractor.
Web Simulation - RelaWavity: Doppler Ellipse - PerSpace-PerSpace β = u/c = 0.866

All the **k**-vectors that are arranged in the lab around a circular protractor as in Fig. 17(a and c) get mapped in the moving frame onto an ellipse as shown in Fig. 17(b and d) with each **k**-origin at the down-**u** focus of the ellipse. The color (frequency $\omega=2\pi\upsilon$) varies with the length $k=|\mathbf{k}|=\omega/c$ of each **k**-vector. This is shown for a dense array of **k**-vectors (one per ° protractor) that form a rainbow when υ falls in the visible spectral region in Fig.18a. There υ-values outside of the visible region are plotted in black. Higher u/c values in Fig. 18b squeeze that color band between an increasing number of black **k** as the enclosing ellipse becomes more eccentric.

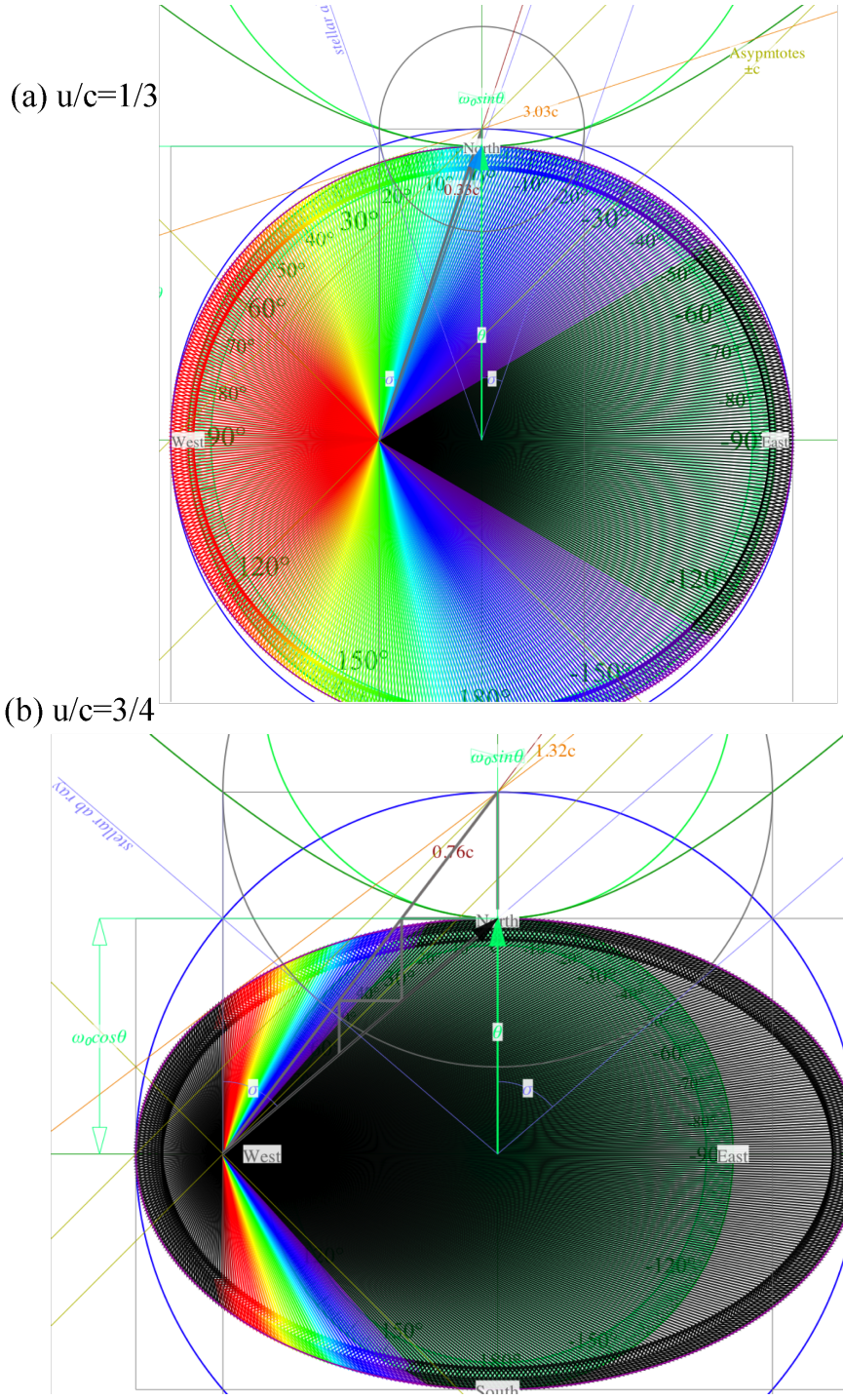

Fig. 18. Dense 2D-array of **k**-vectors of 600THz (blue-green) produces spectrum bounded by infrared and uv.
Web Simulation - RelaWavity: Spectral Ellipse (PerSpace-PerSpace): (a) β = u/c = 1/3 (b) β = u/c = 3/4}

A space-space *(x,y)* array of spherical waves emitted by a moving radiator is shown in Fig. 19. The wavefronts are related to the same **OP′k**-Occam Sword geometry of Fig. 17 and Fig. 18. The oldest spherical wave determines the center of the spectral ellipse an its major axis *2a*. The very youngest (just a dot) determines its primary focus F under the **P′** and **k** vector points that define the small edge of the Occam Sword and focal length $a\varepsilon$ that is the radiator velocity *u*. (Major radius *a* is light velocity *c*.) Stellar aberration ray and its normal wavefront are shown intersecting at **k**. Tangent line T′TT″ contacts spectral ellipse above focus F.

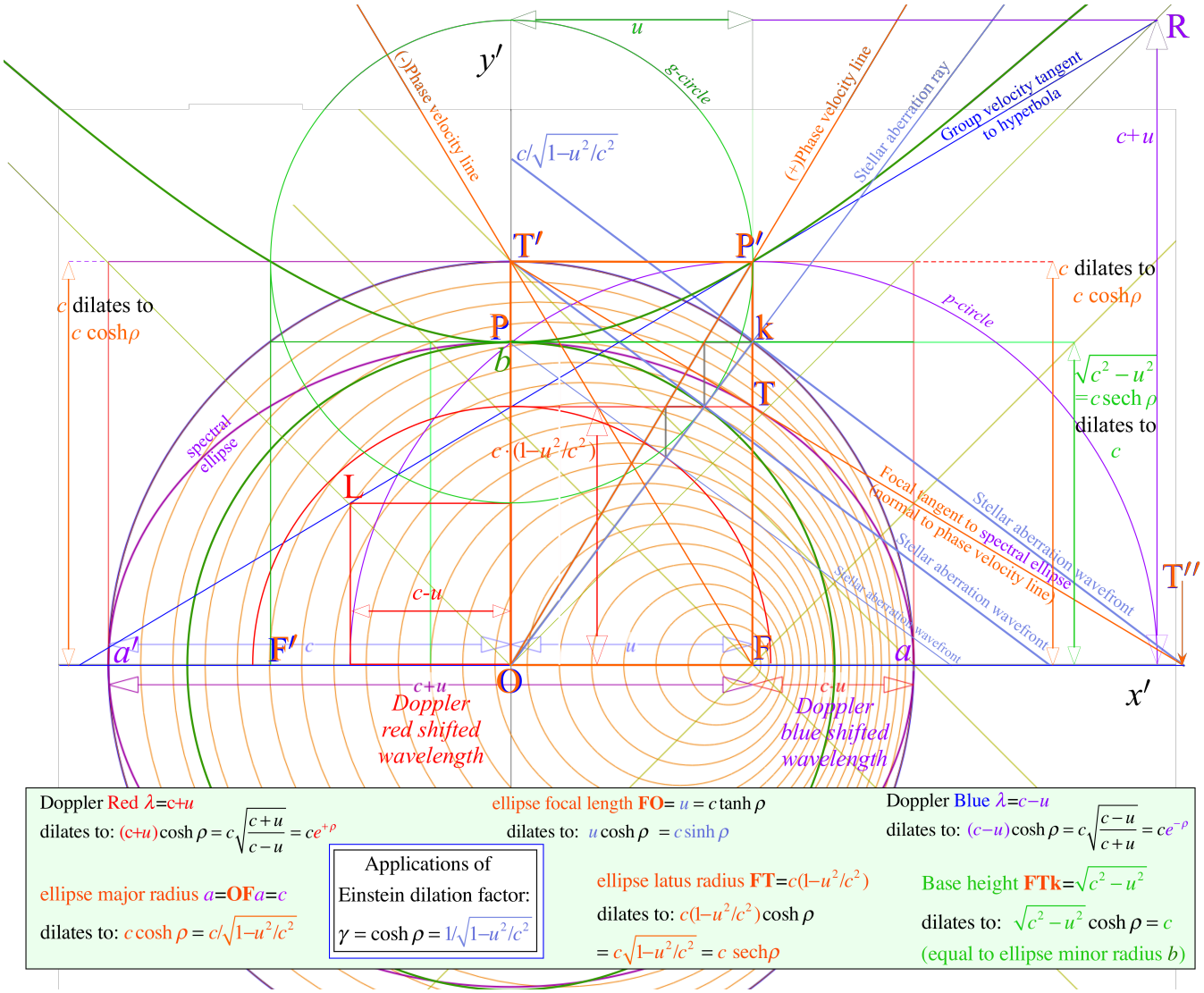

Fig. 19. Occam Sword geometry in space-space involving expanding spherical waves of moving radiator.
Web Simulation - RelaWavity: Wavefronts in Space-Space w/Occam's Sword

The phase dilation factor $\gamma = \cosh\rho = 1/\sqrt{1-u^2/c^2}$ is applied to each of the dimensions listed on Fig. 19 to give results shown in the inset rectangle below the ellipse axis. This results match the Occam Sword dimensions seen in per-space-time *(cκ,υ)*-plot of Fig. 11.